Order Number 9212171

Theoretical study of hydrogen in α-YH_x and on Si(111) surface

Min, Byeong June, Ph.D.

Iowa State University, 1991

U·M·I
300 N. Zeeb Rd.
Ann Arbor, MI 48106

Theoretical study of hydrogen in α-YH_x and on Si(111) surface

by

Byeong June Min

A Dissertation Submitted to the

Graduate Faculty in Partial Fulfillment of the

Requirements for the Degree of

DOCTOR OF PHILOSOPHY

Department: Physics and Astronomy
Major: Solid State Physics

Approved:

Signature was redacted for privacy.

In Charge of Major Work

Signature was redacted for privacy.

For the Major Department

Signature was redacted for privacy.

For the Graduate College

Iowa State University
Ames, Iowa
1991

TABLE OF CONTENTS

LIST OF TABLES

LIST OF FIGURES

ACKNOWLEDGEMENTS

This work was performed at Ames Laboratory under contract no. W-7405-ENG-82 with the U. S. Department of Energy. The United State government has assigned the DOE Report number IS-T1584 to this thesis. I wish to express thanks to Ames Laboratory and the Department of Physics and Astronomy.

I wish to express deep thanks to my advisor Prof. Kai-Ming Ho, whose kind and enthusiastic guidance has been crucial to my completion of the graduate study. I am grateful for Dr. Che-Ting Chan, Dr. Cai-Zhuang Wang, and Prof. Bruce N. Harmon for their guidance and their willingness to share time and knowledge with me.

I thank my wife, Yong Mi, for her patience and encouragement throughout our marriage. My thanks extend to my family here and back in Korea for their support and concern.

Above all, I thank God that He lead me to Jesus Christ during my graduate study while I was still in total rebellion against Him. I thank that He permitted me to finish this graduate work and the wonderful provisions He has bestowed all this time.

CHAPTER 1. INTRODUCTION

Hydrogen in condensed matter has been studied not only for its importance in technological applications but also for its interesting physical and chemical properties. There exists a wide range of possible applications for hydrogen in metals and in semiconductors today [1]. Such include hydrogen embrittlement of metal [2], hydrogen storage in metal [3], and hydrogenation of amorphous semiconductors. On the fundamental side, hydrogen in condensed matter is an interesting problem by itself. Hydrogen is unique in the sense that it is the simplest and the lightest atom in existence and that it has the largest isotope effect. For that reason, hydrogen in condensed matter provides an interesting prototype system for the studies of diffusion [4], adsorption on the surface [5], phase transitions [6], and changes in electronic properties [7].

There has been a great advance in the calculational techniques for evaluating the total energy of solids over the last few decades [8, 9, 10, 11, 12, 13, 14, 15]. It is now possible to calculate the total energy of solids with such an accuracy that the energetics of the solids can be accurately described within the local density approximation(LDA) [16]. The total energy of solids is calculated within the LDA by taking the variational minimum as a functional of the charge density. Since the ground state charge density is not known accurately at the beginning of the calculation, the cal-

culation usually takes on a self-consistent approach, until the difference between the input charge density and the output charge density becomes smaller than a certain criterion. In the frozen core approximation, it is assumed that the nucleus and the core electrons are not responsive to the chemical changes of the environment. Since the energy scale related to usual condensed matter phenomena is many orders of magnitude smaller than the all electron total energy of the atom, higher computational efficiency and better numerical accuracy can be achieved by leaving out the core contributions. Then there is needed an atomic pseudopotential which is capable of simulating an all electron potential. The pseudopotential concept has developed from its original form over a few decades [17]. In our calculations, the pseudopotentials are generated via the norm-conserving scheme [18]. In this scheme, the construction of the atomic pseudopotential does not require the knowledge of core states. However, for the valence states, the pseudowavefunctions should match the all electron wavefunctions accurately outside the core radius, along with the eigenvalues.

Such first-principles total energy calculation techniques have been applied to hydrogen in bcc [11, 12] and fcc [13, 14] metals successfully. In the first part of this thesis, we extend these studies to a hcp metal-hydrogen system. The first-principles total energy calculation has been performed to study the properties of hydrogen in hcp yttrium metal [15]. The results are in good agreement with experiment for many properties of hydrogen in yttrium, such as the equilibrium interstitial location of hydrogen, the heat of formation, the change in the bulk modulus, the lattice expansion upon the solution of hydrogen, and the vibrational frequencies of hydrogen in yttrium. We can also uncerstand better the long range diffusion of hydrogen in yttrium.

Such first-principles total energy calculations have yielded a consistently good description of bulk properties and lattice dynamical properties for a wide range of materials. However, in the case of hydrogen, we should keep in mind the possibility that the light mass of hydrogen may require a quantum mechanical treatment. It is known in many cases that the quantum nature of hydrogen plays a very important role. For example, the zero point motion of hydrogen(and its isotopes) is crucial in understanding the isotope effect for equilibrium hydrogen pressure [19] and phase transition temperatures and pressures [20]. It is apparent that the quantum nature of the hydrogen would have a significant influence on the dynamics of hydrogen. We proceed by assuming that hydrogen is moving in a rigid potential well given by the host metal atoms and solving the Schrödinger equation for hydrogen in the given potential. This includes a Born-Oppenheimer type approximation between the host atoms and the hydrogen, where hydrogen motion is assumed to follow the lattice motion adiabatically. However, since their mass ratio is not that great, the accuracy of the Born-Oppenheimer approximation is still questionable. With the present capacity of computing power, it wouldn't be feasible to treat hydrogen quantum mechanically within the first-principles techniques and it is likely to remain so for a decade or two. In view of this, it is expedient to have an alternate way to describe the energetics of hydrogen by other means than the first-principles total energy calculations. Such an alternate scheme could also be used for a study of very large systems.

With that purpose in mind, we have studied the properties of hydrogen on the Si(111) surface within an empirical tight binding approximation. Even the empirical tight binding models are too involved to describe the hydrogen quantum mechanically at this time. However, with the fast pace of growth in computing power, such

simplified models would be a good first candidate for implementing such ideas in the near future. There are several advantages of a tight binding scheme that make it suitable for an efficient description of the properties of solids. First, it includes the basic features of the electronic structures in the description of the interatomic interaction. As a result, the nature of bonding is described within the quantum mechnical context. Second, it is computationally much less expensive than the first-principles techniques. Third, such savings can be utilized in treating a large system where the first-principles techniques are much too demanding. We will show that an empirical tight binding scheme is efficient and yet accurate enough to be useful for a realistic description of silicon-hydrogen system.

In Chapter 2, the fitting procedure used in the generation of the pseudopotentials and the properties of the pseudopotential used in this calculation is described.

In Chapter 3, the momentum space formalism for the calculation of the total energy of solids under a pseudopotential method is described along with the background information regarding the local density functional approximation. Also the mixed basis approach to self-consistent band structure calculations is presented.

In Chapter 4, these methods are applied to study bulk properties of Y and $YH_{0.5}$. The equilibrium location of hydrogen in Y, equilibrium lattice constants, bulk modulus, cohesive energy, and the heat of formation from our calculation agree well with the experiment.

In Chapter 5, results for the dynamical properties of $YH_{0.5}$ are presented. The hydrogen vibration frequency, splitting of the vibration level, and the activation energy of hydrogen are in good agreement with the experiment.

In Chapter 6, the concept of an empirical tight binding molecular dynamics

simulation is reviewed. Theoretical background for the empirical tight binding scheme and molecular dynamics simulation is discussed.

In Chapter 7, our empirical tight binding model for the Si:H system is presented and the applications are made to the SiH_4 molecule and Si(111):H surface. The hydrogen vibration modes are in excellent agreement with the experiment. The electronic structure from our model is reasonably good.

In Chapter 8, our empirical tight binding scheme is applied in a molecular dynamics simulation. The coupling between the hydrogen vibration modes and the substrate phonon mode is verified. The frequency shift of the hydrogen stretching mode and the anharmonic coupling between the stretching mode and the wagging mode of hydrogen is investigated.

CHAPTER 2. PSEUDOPOTENTIALS

Concepts

The concept of pseudopotentials have developed over a few decades. The early pseudopotential proposed by Phillips and Kleinman [21] was core dependent and its usefuleness was restricted to cases where the pseudopotential was very weak. Computationally, pseudopotentials are easier to deal with since the charge density from a pseudopotential is less sharp than that from the full potential. For this reason, empirical pseudopotential method was developed where the pseudopotential is usually fitted to atomic data [22]. After a process of refining the concept of pseudopotential, the modern pseudopotentials are generated such that they exactly reproduce the all-electron valence orbital outside some core radius. There are usually additional conditions imposed, such as norm-conservation [18] and the smoothness of the potential [23, 24]. Recent efforts are being made in developing softer and more transferable pseudopotentials [25, 26, 27]. In our studies, norm-conserving pseudopotentials are used [18].

Norm-conserving Pseudopotentials

Hamann, Schlüter, and Chiang [18] pointed out that there is no need for the pseudowavefunctions to be orthogonal to the core wavefunctions. Thus it becomes

possible that the pseudopotentials be built without the knowledge of the core states. The major criterion of the norm-conserving pseudopotentials are:

1. The pseudopotential should reproduce the all-electron eigenvalues correctly.

2. The pseudowavefunction should reproduce the all-electron wavefunction outside the core radius r_c.

3. As a consequence, the pseudocharge density ρ_{pseudo} satisfies the following relation with respect to the all-electron charge density ρ_{all} outside r_c.

$$\int_0^r \rho_{pseudo}(\mathbf{r})d\mathbf{r} = \int_0^r \rho_{all}(\mathbf{r})d\mathbf{r}, r \geq r_c, \tag{2.1}$$

4. The logarithmic derivatives of the real and pseudo-wave-function and their first energy derivatives agree for $r > r_c$.

Properties (3) and (4) are crucial for the pseudopotential to have optimum transferability. Property (3) guarantees, through Gauss's theorem, that the electrostatic potential produced outside r_c is identical for the real and pseudocharge distributions.

The norm-conserving pseudopotentials are generated according to the recipe suggested by Hamann, Schlüter, and Chiang [18].

1. An appropriate atomic configuration is chosen as the reference configuration for the construction of the pseudopotential. This configuration does not have to be the ground state configuration. Quite often, excited or even partially ionized configurations are taken as the reference. Self-consistent all-electron calculations are carried out for this reference configuration within the same local density approximation. In our calculation, the Hedin-Lundqvist form is

used consistently [28]. The all-electron valence wavefunction $\psi_l(r)$ and the potential $V(r)$ is obtained.

2. For each valence state l, the potential is constructed in the form:

$$V_{1,l}(r) = V(r)[1 - f(r/r_{cl})] + c_l f(r/r_{cl}), \tag{2.2}$$

where r_{cl} is the cutoff radius for each l. The restrictions are that $f(x)$ is a smooth "cutoff function" which approaches 0 as $x \rightarrow \infty$, approaches 1 at least as fast as x^3 as $x \rightarrow 0$, and cuts off for $x \sim 1$. The constant c_l is adjusted so that the nodeless solution w_{1l} of the radial Schrödinger equation with V_{1l} has energy ϵ_{1l} equal to the original eigenvalue ϵ_l. This potential converges to $V(r)$ for $r > r_{cl}$.

Property (1) of the last section being thus satisfied, the normalized function w_{1l} satisfies property (2) within a multiplicative constant,

$$w_{1l}(r) = \gamma_l u_l(r), \ \ for\ r > r_c, \tag{2.3}$$

where $u_l(r) = r\psi(r)$.

3. The pseudowavefunction $w_{2l}(r)$ is constructed from $w_{1l}(r)$ by

$$w_{2l}(r) = \gamma_l[w_{1l}(r) + \delta_l g_l(r/r_{cl})], \tag{2.4}$$

where $g_l(x)$ cuts off to zero for $x > 1$, and behaves as x^{l+1} at small x. The chosen asymptotic behavior of $f(x)$ and $g(x)$ guarantees the potential to be finite at the origin. The choice of cutoff functions used by Hamann, Schlüter, and Chiang is $f(x) = exp(-x^c)$, and $g_l(x) = x^{l+1}exp(-x^c)$ where c is varied in the fitting to assure the pseudowavefunction $w_{2l}(r)$ is a smooth function. The

δ_l is determined by the smaller solution of the quadratic equation resulting from the normalization requirement of the wave function:

$$\gamma_l^2 \int_0^\infty [w_{1l}(r) + \delta_l g_l(r/r_{cl})]^2 dr = 1 \tag{2.5}$$

4. The final screened pseudopotential V_{2l} defined as that potential which produces the nodeless pseudo-orbital w_{2l} with eigenvalue $\epsilon_{2l} = \epsilon_k$, is found by inverting the radial Schrödinger equation. The result is given by:

$$\begin{aligned} V_{2l}(r) &= V_{1l}(r) + [\frac{1}{w_{2l}(r)} \frac{d^2}{dr^2} w_{2l}(r) - \frac{1}{w_{1l}(r)} \frac{d^2}{dr^2} w_{1l}(r) \qquad (2.6) \\ &= \frac{\delta_l g_l(r/r_c)}{w_{1l}(r) + \delta_l g_l(r/r_c)} [\epsilon_l - V_{1l}(r) - \frac{l(l+1)}{r^2} \\ &\quad + \frac{1}{g_l(r/r_c)} \frac{d^2 g_l(r/r_c)}{dr^2}] + V_{1l}(r). \end{aligned}$$

5. Finally the ionic pseudopotential $V_{ps,l(r)}$ is obtained by unscreening $V_{2l}(r)$:

$$V_{ps,l}(r) = V_{2l}(r) - (V_H(r) + V_{xc}(r)), \tag{2.7}$$

where $V_H(r)$ and $V_{xc}(r)$ are the Hartree and the exchange correlation potential, respectively, which can be calculated from the pseudocharge distribution.

Application to Y

Within the norm-conserving scheme, a non-local ionic pseudopotential was built for transition metal element Y (Figure 2.1). The relativistic Dirac equation [29] for the Y atom was solved for the all-electron atomic eigenvalues, wavefunctions, and the total energies. Atomic configurations with excitation energies less than 1 Ry were considered. Since the 4p electrons are located farther away from the nucleus, they

are sensitive to the configuration of the atom. Thus it is best to treat 4p electrons as valence electrons to achieve good core-valence separation and to improve the transferability of the pseudopotential to different surroundings. Compared with the partial core correction scheme [30], this approach is simpler and more straightforward in its physical concept. The quality of the pseudopotential can be examined by comparing the eigenvalues and the excitation energies from the pseudoatom calculations with the all-electron calculation results (Table 2.1). In most cases, the eigenvalues and the excitation energies are reproduced within 0.01 Ry with respect to the all-electron results.

Table 2.1: The Y pseudopotential eigenvalues and the excitation energies compared with the all-electron self-consistent calculation results(in parantheses)

Configuration	Eigenvalues 4d	5s	5p	Excitation energy (Ry)
$4d^1 5s^2$	-0.2002	-0.3180	-0.1189	0
	(-0.2005)	(-0.3174)	(-0.1157)	0
$4d^2 5s^1$	-0.1335	-0.2881	-0.1035	0.1398
	(-0.1351)	(-0.2853)	(-0.1010)	(0.1350)
$4d^1 5s^1 5p^1$	-0.2654	-0.3665	-0.1583	0.2034
	(-0.2718)	(-0.3681)	(-0.1564)	(0.2065)
$5s^2 5p^1$	-0.3717	-0.4090	-0.1831	0.1322
	(-0.3748)	(-0.4140)	(-0.1793)	(0.1372)
$4d^3$	-0.1022	-0.2759	-0.1014	0.3066
	(-0.1022)	(-0.2700)	(-0.0980)	(0.2957)
$5s^1 5p^2$	-0.4290	-0.4488	-0.2141	0.3635
	(-0.4431)	(-0.4578)	(-0.2123)	(0.3774)
$4d^1 5p^2$	-0.3237	-0.4082	-0.1903	0.4186
	(-0.3369)	(-0.4118)	(-0.1895)	(0.4235)
$4d^2 5p^1$	-0.1933	-0.3353	-0.1420	0.3307
	(-0.1983)	(-0.3330)	(-0.1401)	(0.3234)
$5p^3$	-0.4807	-0.4841	-0.2414	0.6022
	(-0.5063)	(-0.4967)	(-0.2415)	(0.6278)

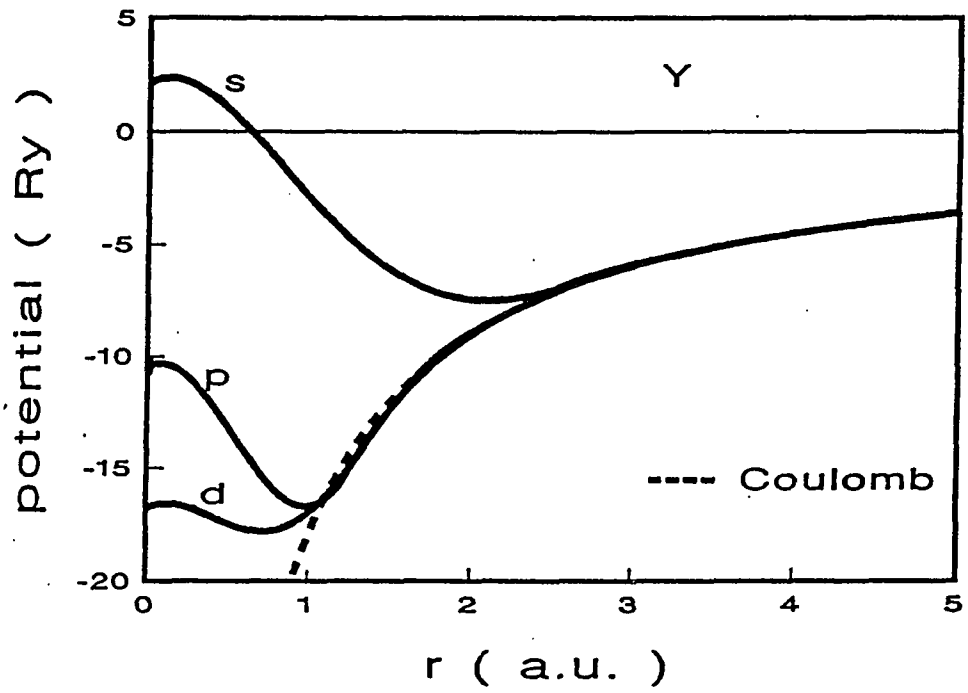

Figure 2.1: The angular momentum-dependent pseudopotential for yttrium shown with the Coulomb potential(dotted line)

CHAPTER 3. TOTAL ENERGY CALCULATION IN SOLIDS

Local Density Functional Theory

The many-electron problem in solids is so complicated that it cannot be tackled without simplification. Usually it is reduced to a one-electron problem where the many-body interactions are represented by an effective one-electron potential. There are numerous schemes to achieve that goal, such as the Hartree approximation, the Hartree-Fock approximation, and the local density functional approximation. Among those schemes, the local density functional (LDF) approach has been particularly successful in the electronic structure and the total energy calculation of solids. This approach is based on the Hohenberg-Kohn theorem [16]. The Hohenberg-Kohn theorem can be summarized as follows:

1. The ground state energy of a system of identical fermions is a unique functional of the particle density.

2. This functional has its minimum value at the correct charge density $\rho(\mathbf{r})$ with respect to variation of the particle density subject to the constraint of particle number conservation.

Unlike Hartree-Fock type approximations, the basic variable in the local density functional approximation is the electron density instead of the electron wavefunction.

Within the LDF, the total energy can be written as (in atomic units)

$$E_T[\rho(\mathbf{r})] = T[\rho] + E_H[\rho] + E_{xc}[\rho(\mathbf{r}] + E_{e-i} + E_{i-i}, \tag{3.1}$$

$$E_H = \frac{1}{2}\int\int \frac{\rho(\mathbf{r})\rho(\mathbf{r}')}{|\mathbf{r}-\mathbf{r}'|}d\mathbf{r}d\mathbf{r}'$$

$$E_{e-i} = \int V(\mathbf{r})\rho(\mathbf{r})d\mathbf{r}$$

where $T[\rho]$ is the electronic kinetic energy, $E_H[\rho]$ is the electronic Hartree energy, $E_{xc}[\rho(\mathbf{r})]$ is the exchange-correlation energy, E_{e-i} is the electron-ion interaction energy with $V(\mathbf{r})$ describing the ionic potential, and E_{i-i} is the ion-ion interaction energy.

From the variational principle, we have a set of coupled one-particle equations

$$[-\nabla^2 + V_{eff}]\psi_i(\mathbf{r}) = \epsilon_i\psi_i(\mathbf{r}) \tag{3.2}$$

$$\rho(\mathbf{r}) = \sum_{i=1}^{N} n_i|\psi_i(\mathbf{r})|^2,$$

where n_i is the occupation number of the state i, and N is the total number of electrons in the system, and V_{eff}, is the effective potential

$$\begin{aligned} V_{eff}[\rho(\mathbf{r})] &= V(\mathbf{r}) + V_H(\mathbf{r}) + V_{xc}(\mathbf{r}) \\ &= V(\mathbf{r}) + \int \frac{2\rho(\mathbf{r}')}{|\mathbf{r}-\mathbf{r}'|}d\mathbf{r}' + \frac{\delta(E_{xc}[\rho(\mathbf{r})])}{\delta\rho(\mathbf{r})}, \end{aligned}$$

Then $T[\rho]$, the kinetic energy of non-interacting particles with the same density, can be written as

$$T[\rho] = \sum_i n_i < \psi_i| - \nabla^2|\psi_i > .$$

The exchange-correlation energy functional is approximated by

$$E_{xc}[\rho(\mathbf{r})] = \int d\mathbf{r}\varepsilon_{xc}(\rho(\mathbf{r}))\rho(\mathbf{r}),$$

where $\varepsilon_{xc}(\rho(\mathbf{r}))$ is the exchange-correlation energy adapted from the uniform electron gas. $\varepsilon_{xc}(\rho(\mathbf{r}))$ is not known exactly, but approximations such as the Wigner interpolation formula [31], Hedin-Lundqvist local exchange-correlation potential [28], and an analytical fit to Ceperley and Alder's Monte Carlo results [32] are often used. The Hedin-Lundqvist formulation is used throughout the present study.

These equations are solved self-consistently until the difference between the input charge density and the output charge density becomes smaller than some criterion. With the charge density determined thus, the ground state properties of the system can be obtained.

Momentum Space Formalism for the Total Energy of Solids

The total energy calculation is greatly simplified by using a momentum space expression derived by Ihm, Zunger, and Cohen [33]. There is no further shape approximation or multicenter integrals within this formulation. This makes it suitable for use with the self-consistent pseudopotential method. For non-overlapping ionic cores, Equation 3.1 becomes

$$\begin{aligned} E_T &= \sum_i n_i < \psi_i | - \nabla^2 | \psi_i > + \frac{1}{2} \int \int \frac{2\rho(\mathbf{r})\rho(\mathbf{r}')}{|\mathbf{r}-\mathbf{r}'|} d\mathbf{r} d\mathbf{r}' \\ &+ \int \rho(\mathbf{r}) \varepsilon_{xc}(\rho(\mathbf{r})) d\mathbf{r} + \sum_{\mathbf{R},\tau} \int \rho(\mathbf{r}) V_{ps}^{L}(\mathbf{r}-\mathbf{R}-\tau) d\mathbf{r} \\ &+ \sum_{\mathbf{R},\tau} \sum_{i,l} n_i < \psi_i | V_{ps,l}^{NL}(\mathbf{r}-\mathbf{R}-\tau) \hat{P}_l | \psi_i > + \frac{1}{2} \sum_{\mathbf{R},\mathbf{R}',\tau,\tau'}^{\prime} \frac{2Z_v^2}{|\mathbf{R}+\tau-\mathbf{R}'-\tau|}, \end{aligned} \tag{3.3}$$

where the prime in the summation excludes the $|\mathbf{R}+\tau-\mathbf{R}'-\tau'|=0$ term, $\mathbf{R},\mathbf{R}'$ denote the lattice translation vectors, τ,τ' denote the basis vectors, Z_v is the ionic charge, and V_{ps}^L is the local part of the pseudopotential common to all angular momentum components of the wavefunction. The non-local part is defined by

$$V_{ps,l}^{NL}(\mathbf{r}) = V_{ps,l}(\mathbf{r}) - V_{ps}^L(\mathbf{r}),$$

where $V_{ps,l}$ is the angular momentum dependent pseudopotential and $\hat{P}_l$ is the projection operator for the angular momentum l. This separation makes only the local pseudopotential V_{ps}^L include the long-range interaction, thereby making the non-local parts $V_{ps,l}^{NL}$ short-ranged. This procedure is always possible since $V_{ps,l} \sim -2Z/r$ for any l for large r.

The total energy expression can be further simplified in terms of the electron eigenvalues determined from the band structure calculation. From Equation 3.2,

$$[-\nabla^2 + V_{eff}]\psi_i(\mathbf{r}) = \epsilon_i\psi_i(\mathbf{r}),$$

is now written with

$$V_{eff} = \sum_{\mathbf{R},\tau}[V_{ps}^L(\mathbf{r}-\mathbf{R}-\tau) + \sum_l V_{ps,l}^{NL}(\mathbf{r}-\mathbf{R}-\tau)\hat{P}_l] + V_H^{in}(\mathbf{r}) + V_{xc}^{in}(\mathbf{r}),$$

where V_H^{in} is the input Hartree potential, and V_{xc}^{in} is the input exchange-correlation potential from the input charge density, in a self-consisitent band structure calculation. Equation 3.2 is multiplied by $\psi_i^*(\mathbf{r})$, integrated over $\mathbf{r}$, and summed over i, and the result is substituted into Equation 3.4. Then the total energy per primitive unit cell is

$$E_T = 2\sum_{n\mathbf{k}}^{(occ.)} w_{\mathbf{k}}\epsilon_{n\mathbf{k}} + \frac{1}{2}\sum_{\mathbf{r},\tau,\tau'}\frac{2Z_v^2}{|\mathbf{R}+\tau-\tau'|}$$

$$- \Omega_{cell}[\frac{1}{2}\sum_{\mathbf{G}}\frac{8\pi|\rho(\mathbf{G})|^2}{|\mathbf{G}|^2} + \sum_{\mathbf{G}}\rho(\mathbf{G})(\epsilon_{xc}(\mathbf{G}) - V_{xc}^{in}(\mathbf{G}))]$$

where $w_{\mathbf{k}}$ is the weight of the sampled k-point, n is the band index, Ω_{cell} is the volume of the primitive unit cell, and G denotes the reciprocal lattice vector.

Since the Coulomb interaction is also long-ranged, $V_{ps}(\mathbf{G}=0)$, $E_H(\mathbf{G}=0)$, and E_{i-i} are also divergent. These divergent terms, however, should sum up to a finite number because of the charge neutrality. This quantity can be evaluated by employing the Ewald technique [34]. Thus the band structure calculation can be done by setting $V_{ps}(\mathbf{G}=0)=0$ and $V_H(\mathbf{G}=0)=0$. This constant shift is then compensated when calculating the E_{i-i} term. As a result, the Equation 3.4 can be rewritten finally as

$$\begin{aligned} E_T &= 2\sum_{n\mathbf{k}}^{(occ.)} w_{\mathbf{k}}\epsilon_{n\mathbf{k}} + \alpha_1 Z_v + \gamma_{Ewald} \\ &- \Omega_{cell}[\frac{1}{2}\sum_{\mathbf{G}\neq 0}\frac{8\pi|\rho(\mathbf{G})|^2}{|\mathbf{G}|^2} + \sum_{\mathbf{G}}\rho(\mathbf{G})(\epsilon_{xc}(\mathbf{G}) - V_{xc}^{in}(\mathbf{G}))], \end{aligned} \tag{3.4}$$

where the divergent G=0 terms and the ion-ion interaction energy are evaluated together in the $\alpha_1 Z_v + \gamma_{Ewald}$ term. Then γ_{Ewald} is the Coulomb interaction energy of the ion cores immersed in the neutralizing homogeneous charge density and α_1 is given by

$$\alpha_1 = \frac{N_a}{\Omega_{at}}\int(V_{ps}^L(\mathbf{r}) + \frac{2Z_v}{r})d\mathbf{r},$$

where N_a is the number of atoms per primitive cell and Ω_{at} is the atomic volume.

Mixed-basis Approach to Electronic Structure Calculations

In most band theoretical methods, the electronic wavefunction is expanded in a set of basis functions and the solution of the Schrödinger equation is obtained by a variational procedure. It is of critical importance to choose a small, yet physically complete, set of basis functions.

It would require a huge basis set in order to treat a system which exhibits atomic-like character as well as extended plane wave-like character. This problem can be solved by employing an energy independent basis set consisting of both plane waves and a Bloch sum of localized orbitals for the expansion of the electronic wave function [35]

$$\psi_{n\mathbf{k}}(\mathbf{r}) = \frac{1}{\sqrt{\Omega}}\sum_{\mathbf{G}}\alpha_n(\mathbf{k}+\mathbf{G})e^{i(\mathbf{k}+\mathbf{G})\cdot\mathbf{r}} + \sum_{jm}\beta_{jm}(n,\mathbf{k})\phi_{jm}(\mathbf{k},\mathbf{r}), \qquad (3.5)$$

with

$$\phi_{jm}(\mathbf{k},\mathbf{r}) = \frac{1}{\sqrt{N}}\sum_{\mathbf{R}} e^{\mathbf{k}\cdot(\mathbf{R}+\tau_j)} f_{jm}(\mathbf{r}-\mathbf{R}-\tau_j),$$

where Ω is the crystal volume, N is the number of atoms, and m is the label for the orbital on the j^{th} atom.

In the present study, local orbitals of the form

$$f_{lm}(\mathbf{r}) = Nr^l exp(-\gamma r^s)Y_{lm}(\theta,\phi),$$

are used for Y to augment the 4p and 4d electronic states, where N is the normalization constant, and l, m are angular momentum quantum numbers. For H, a numerical local orbital is constructed from the H pseudowavefunction by multiplying a cutoff function of the form

$$f_{cut}(r) = 1 - exp(-\alpha(r_c - r)^2),$$

where r_c is the cutoff radius and α is to be determined variationally. Since charge density around an atom in a condensed matter system is usually quite close to the atomic charge density, such numerical basis functions can effectively augment the plane wave basis set.

This mixed basis set leads to the following matrix eigenvalue problem:

$$(H - ES)\Lambda = 0, \tag{3.6}$$

where H is the Hamiltonian matrix, S is the overlap matrix, and Λ is a column vector with elements λ_1,...,λ_n corresponding to the expansion coefficients α, β in equation 3.5. When evaluating the matrix elements involving the local orbital, if we are using the Gaussian as local orbital we make use of the on-site approximation [35], but when using the numerical basis, the on-site approximation becomes exact if r_c is smaller than the nearest-neighbor distance.

The valence charge density is then calculated from

$$\rho(\mathbf{r}) = 2\sum_{n\mathbf{k}} \theta(\epsilon_f - \epsilon_{n\mathbf{k}})|\psi_{n\mathbf{k}}(\mathbf{r})|^2, \tag{3.7}$$

where $\theta(x)$ is the step function and ϵ_f is the Fermi energy and is determined from the number of electrons per primitive cell, z, by the equation:

$$z = 2\sum_{n\mathbf{k}} \theta(\epsilon_f - \epsilon_{n\mathbf{k}}). \tag{3.8}$$

In practice, the k summation is restricted to the irreducible part of the Brillouin zone (IBZ) and the charge density is symmetrized such that the output charge density would have the correct symmetry.

Procedure for Self-consistent Calculation

The total energy expression in Equation 3.5 can be arranged in an especially suitable form for a self-consistent calculation:

$$E_T = 2\sum_{n\mathbf{k}}^{(occ.)} w_{\mathbf{k}}\epsilon_{n\mathbf{k}} - \Omega_{cell}\sum_{\mathbf{G}}\rho(\mathbf{G})V_{sc}^{in}(\mathbf{G}) + \Omega_{cell}\frac{1}{2}\sum_{\mathbf{G}\neq 0}\frac{8\pi|\rho(\mathbf{G})|^2}{|\mathbf{G}|^2} + \Omega_{cell}\sum_{\mathbf{G}}\rho(\mathbf{G})\epsilon_{xc}(\mathbf{G}) + \alpha_1 Z_v + \gamma_{Ewald},$$

where

$$V_{sc}^{in}(\mathbf{G}) = \frac{8\pi\rho(\mathbf{G})}{|\mathbf{G}|^2} + V_{xc}^{in}(\mathbf{G}).$$

Then the calculation proceeds as follows:

1. The Equation 3.6 is solved for the eigenvalues and the eigenfunctions within the mixed basis approach with an input screening potential V_{xc}. Before the iteration starts, the plane wave cutoff energy, Gaussian coefficients, and the cutoff functions are optimized for best convergence.

2. The Fermi level is determined and the occupation of each state is calculated via Equation 3.8. For metal systems with partially filled bands at the Fermi level, accurate determination of the Fermi surface requires many k-points. The Gaussian smearing method is used to accelerate k-point sampling of the IBZ [11]. In this scheme, each eigenvalue is replaced by a Gaussian of a certain width, which is roughly equal to the dispersion of the energy bands between neighboring grid points near the Fermi surface. This scheme is convenient to use and very efficient. Then the Fermi level is determined from the Gaussian

broadened density of states:

$$\begin{aligned} z &= \sum_{n\mathbf{k}} f_{n\mathbf{k}} \\ &= w_{\mathbf{k}} \int_{-\infty}^{E_F} \frac{2}{\sqrt{\pi}\delta} exp[-(\frac{\varepsilon - \varepsilon_{n\mathbf{k}}}{\delta})^2] d\varepsilon, \end{aligned}$$

where δ is the Gaussian width, and $f_{n\mathbf{k}}$ represents the occupation of the state $(n, \mathbf{k})$.

3. The total charge density is calculated according to Equation 3.7 and symmetrized. The Hartree potential V_H and the exchange correlation potential V_{xc} are calculated from the total charge density. The new screening potential is usually constructed by mixing the input screening potential and the output screening potential by

$$V_{in}^{new}(\mathbf{G}) = cV_{in}^{old}(\mathbf{G}) + (1-c)V_{out}^{old}(\mathbf{G}),$$

where the mixing coefficient c is a function of $|\mathbf{G}|$ which corresponds to screening the charge density oscillation by a Thomas-Fermi type dielectric function.

4. The total energy is calculated according to Equation 3.5 until the self-consistency is attained where the total energy is stable within 10^{-5} Ry or less, corresponding to a self-consistency error of 10^{-4} Ry or less between the input and output screening potentials in reciprocal space.

CHAPTER 4. BULK PROPERTIES OF Y AND α-$YH_{0.5}$

Yttrium has the ground state atomic configuration of [Kr]$4d^1 5s^2$ and its low temperature phase is in the regular hexagonal closed packed structure with a c/a ratio which is within 3% of the ideal value $\sqrt{8/3}$. Recently yttrium has attracted attention for its unusual behavior when hydrogen is added. There has been a controversy over the location of hydrogen impurities in yttrium metal [36, 37, 38, 39] until very recently. The maximum solubility of hydrogen in α-YH_x is about $x = 0.5$ at 900 K [40]. The disordered α-phase seems to extend down to zero temperature without precipitation (0.245 H/Y at 4 K) [39], in contrast to vanishing concentration in the case of the bcc and fcc metals. It is also known that the anharmonic effects are important in the vibration of hydrogen. [53]. All these suggest that the behavior of hydrogen in hcp metals is drastically different than in the bcc or fcc metals.

The total energy calculation of Y and α-$YH_{0.5}$ is performed with the Y pseudopotential generated according to the norm conserving pseudopotential procedure described in Chapter 2. A mixed basis set of plane waves and Bloch sums of localized orbitals are used in the expansion of the electronic wavefunctions. Our basis consists of plane waves up to the cutoff energy $E_{cut} = 10.5$ Ry (approximately 125 waves per atom), supplemented by two sets of local orbitals of the form

$$f_{lm} = N r^l exp(-\gamma r^s) Y_{lm}(\theta, \phi).$$

The values for γ are determined to maximize the convergence of the basis set of the local orbitals and the plane waves. We use $l = 1, s = 3$, and $\gamma = 0.420$ a.u. for the $4p$ electrons, and $l = 2, s = 2$, and $\gamma = 0.892$ a.u. for the $4d$ electron after the optimization. In the case of the bulk yttrium metal, the energy eigenvalues and the wave functions are calculated at 60 k points inside the irreducible Brillouin zone (IBZ).

The total energy of bulk yttrium has been calculated as a function of the lattice volume for the hcp, bcc, and fcc structures. The equilibrium atomic volume for the hcp structure is calculated to be 211 a.u. at the ideal c/a ratio of 1.633, in good agreement with 223 a.u. of experiment [42]. The c/a ratio is determined to be 1.57 at this atomic volume, giving the equilibrium lattice constants a=3.58 $\AA$, c=5.63 $\AA$ (Figure 4.1). The experiments report a=3.65 $\AA$, c=5.73 $\AA$, giving c/a=1.57 [42]. Also, the total energies of the yttrium metal in bcc and fcc structures versus the atomic volume are calculated. The results are fitted to the universal binding curve [43]

$$E(r) = E_0(1 + x)e^{-x}, x = (r - r_0)/l,$$

where E_0, r_0, and l are scaling parameters. By comparing the value of E_0 with the free atom energy of Y, we calculate the cohesive energy of bulk yttrium. In determining the free atom energy of Y, we include the spin polarization energy adapted from a spin polarized atomic calculation. The results are shown in Figure 4.2. It is easily seen from the picture that the hcp structure is energetically most favorable. Our result predicts a phase transition from the hcp phase to the fcc phase at high pressure, which should correspond to the slope of the common tangent line to the hcp curve and the fcc curve. We get 44 kbar for such a transition pressure. The high pressure

x-ray diffraction experiments [44, 45] report a series of phase transitions from hcp → Sm-type → dhcp → fcc structures. The transition to the Sm-type, dhcp, and fcc structures occur at around 100, 250, and 460 kbar, respectively. Comparison with our calculation is complicated by the presence of the intermediate crystal phases, but the data indicate that our transition pressure is too small by a factor of about 2.5. One possible explanation may be that we have kept the c/a ratio constant in the hcp structure as we change the volume. Relaxation of the c/a ratio will lower the small volume portion of the hcp versus volume curve and hence increase the calculated transition pressure. Further calculations to verify this idea increase the transition pressure only by 10 %. Thus, it appears we cannot predict the transition pressure from our present calculation.

From the curvature of the universal binding curve, we get 0.45 Mbar for the bulk modulus. Scott [46] reports 0.42 Mbar. For an accurate determination of the cohesive energy, the number of plane waves in the expansion of the wave function is increased and the cohesive energy is fitted as a function of the cutoff energy in a form

$$E_{coh} = \frac{\lambda}{E_{cut}^4 + \mu} + E_{coh}^0,$$

with three parameters λ, μ, and E_{coh}^0 (Figure 4.3). The extrapolated cohesive energy is E_{coh}^0=0.348 Ry/atom compared to 0.325 Ry/atom from the experiment.

The density of states is calculated by sampling 2448 k points within the irreducible Brillouin zone. The eigenvalues are broadened into a Gaussian. For the width of the Gaussian, three values have been tried, 0.05, 0.08, and 0.1 eV. We have $N(E_F)$=1.92 electrons/Y atom eV. This value of $N(E_F)$ is independent of the Gaussian width used. The result is shown in Figure 4.4. The shape of the density of

states and the value of $N(E_F)$ are in good agreement with the photoemission study of Eastman [47]. The results are summarized in Table 4.1 with other theoretical values [10, 48] and the experimental results.

For a study of α-phase YH_x, we consider the $YH_{0.5}$ primitive unit cell in the hcp structure (as is shown in Figure 5.1). It is assumed that the hydrogen-hydrogen interaction will not be large enough to affect the bulk properties significantly. We have calculated the total energy of $YH_{0.5}$ to determine the equilibrium interstitial location of H atom and the lattice constant changes on addition of hydrogen into the yttrium host. It turns out that the octahedral site is higher in energy by 104 meV per $YH_{0.5}$ primitive unit cell than the tetrahedral site. Preliminary investigations of the zero point energy shows that the zero point energy at the octahedral site, having more space about itself, is smaller than the zero point energy at the tetrahedral site by 70 meV. This difference is not enough to reverse the tetrahedral site occupancy of hydrogen. This agrees with a recent inelastic neutron scattering experiment [36].

Having established the tetrahedral site occupancy of hydrogen in yttrium, other bulk properties of $YH_{0.5}$ are calculated with the hydrogen fixed at the tetrahedral site. It is found that the volume of the hcp $YH_{0.5}$ primitive unit cell increases to 231 a.u. and the c/a ratio also increases to 1.62. This translates to lattice constants a=3.65 $\AA$, c= 5.93 $\AA$. Beaudry and Spedding [49] report a=3.66 $\AA$, c= 5.79 $\AA$, with c/a=1.58 at the concentration of 19.0 at. % H. If we assume the lattice constant variation is linear in hydrogen concentration as is generally thought, then our result would correspond to a=3.61 $\AA$, c= 5.74 $\AA$, with c/a=1.59 at the concentration of 19.0 at. % H. The density of states of $YH_{0.5}$ is shown in Figure 4.5. $N(E_F)$ is 1.38 electrons/Y atom eV. We have sampled 4624 k points within the irreducible Brillouin

zone.

The heat of formation of $YH_{0.5}$ is calculated by considering the total energy difference of $YH_{0.5}$ and the bulk Y + atomic H. The same cutoff energies for the plane wave basis are used for $YH_{0.5}$ and bulk Y to maximize the cancellation of errors. The total energy of $YH_{0.5}$ with respect to the total energy of the bulk Y + atomic H as a function of the cutoff energy is fitted to the same form as in the bulk Y case (Figure 4.6). We have 3.20 eV per hydrogen atom as the cohesive energy of $YH_{0.5}$ with respect to the bulk Y + atomic H. We use the binding energy of molecular hydrogen calculated by Gunnarson and Johansson [50] and consider the zero point energies of hydrogen both in bulk Y and in molecular hydrogen, to determine the heat of formation 0.74 eV per hydrogen atom, or 8500 cal/g atom of $YH_{0.5}$. This is in good agreement with the value 7746 cal/g atom of $YH_{0.5}$ measured by Yannopoulos, Edwards, and Wahlbeck [51]. Again the results for the $YH_{0.5}$ are fitted to the universal binding curve and the bulk modulus now increases to 0.55 Mbar.

Conclusion

We have performed first-principles total energy calculations for Y metal and $YH_{0.5}$ to investigate their bulk properties. Our results for the equilibrium lattice constants, cohesive energy, and the bulk modulus of Y metal are in excellent agreement with the experiment. We have established that the hydrogen occupies the tetrahedral sites of hcp Y metal. We have also obtained a reasonable description of the lattice expansion, the c/a ratio change, and the heat of formation as the hydrogen is dissolved. The good agreement between our result and the experiments provides encouragement for further investigations of the yttrium-hydrogen systems.

Table 4.1: Main results of our calculation on Y compared with experiments and other theoretical calculations. Moruzzi et al assume the fcc structure

	Present calculation	Moruzzi *et al* [10]	Loucks [48]	experiment
Atomic volume (a.u.)	211	197	223	223
c/a-ratio	1.57		1.58	1.57
cohesive energy (Ry/atom)	0.348	0.362		0.325
bulk modulus (Mbar)	0.45	0.33		0.42
$N(E_F)$ (electrons/eV atom)	1.86	1.41	1.97	1.67

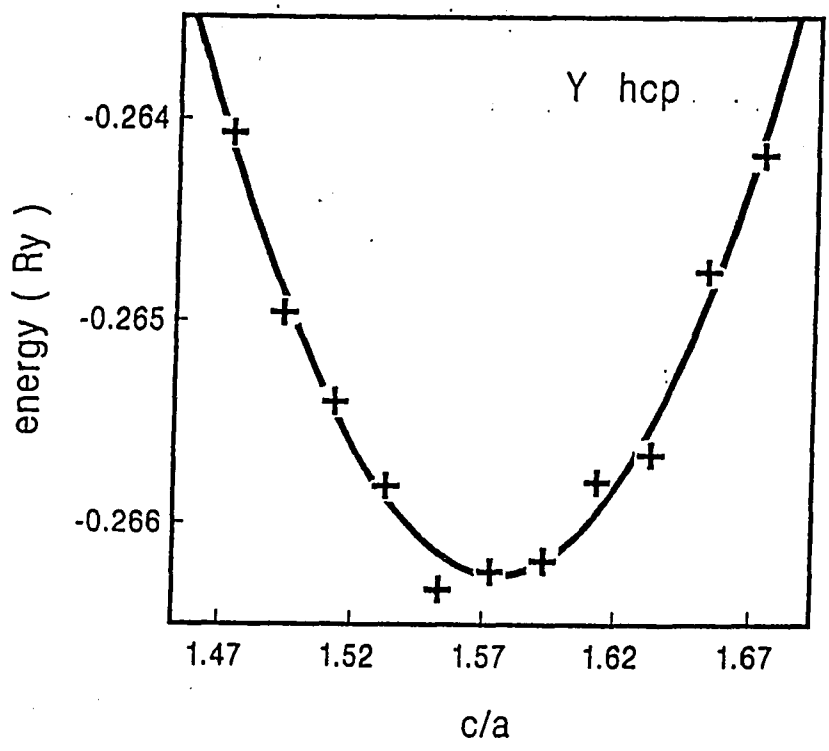

Figure 4.1: The total energy of hcp Y metal is calculated for different c/a ratios (+) at the atomic volume of 211 a.u. The curve is the least squares fit to a parabola, which gives the equilibrium ratio 1.57

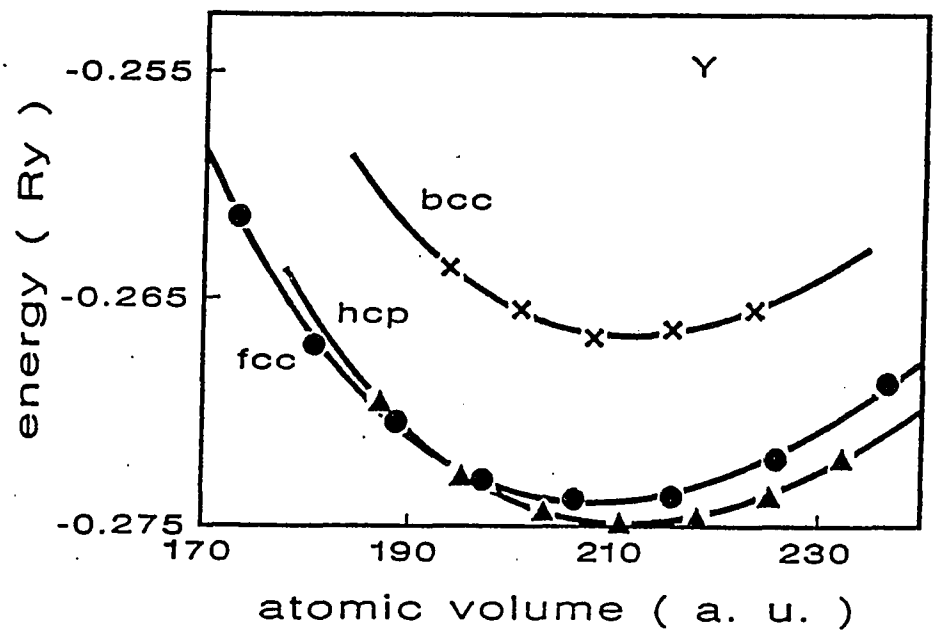

Figure 4.2: The cohesive energy of bulk Y versus atomic volume for different lattice structures. The hcp curve is taken at c/a=1.57

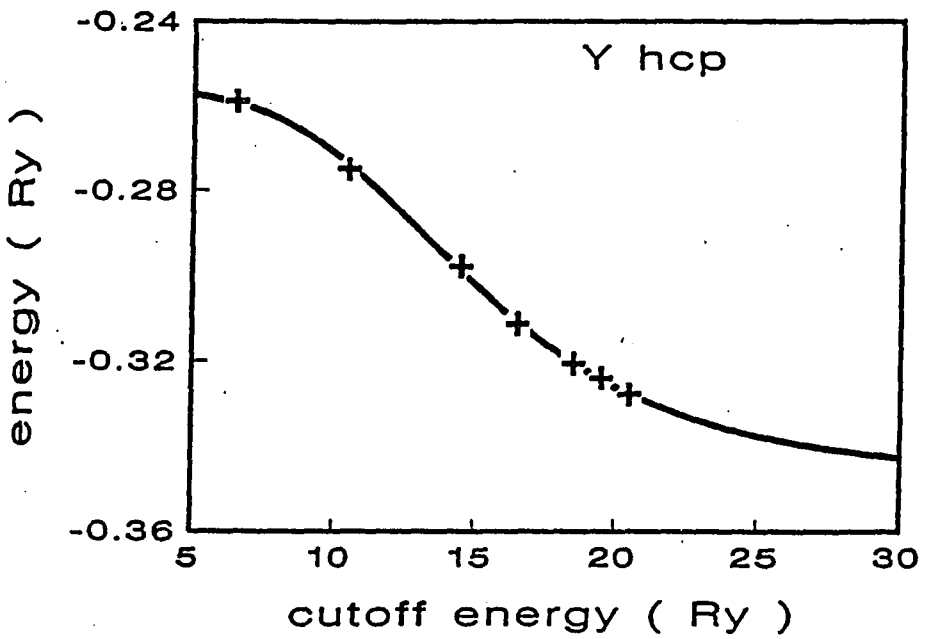

Figure 4.3: The convergence of the cohesive energy of bulk Y as a function of cutoff energy for the plane wave basis

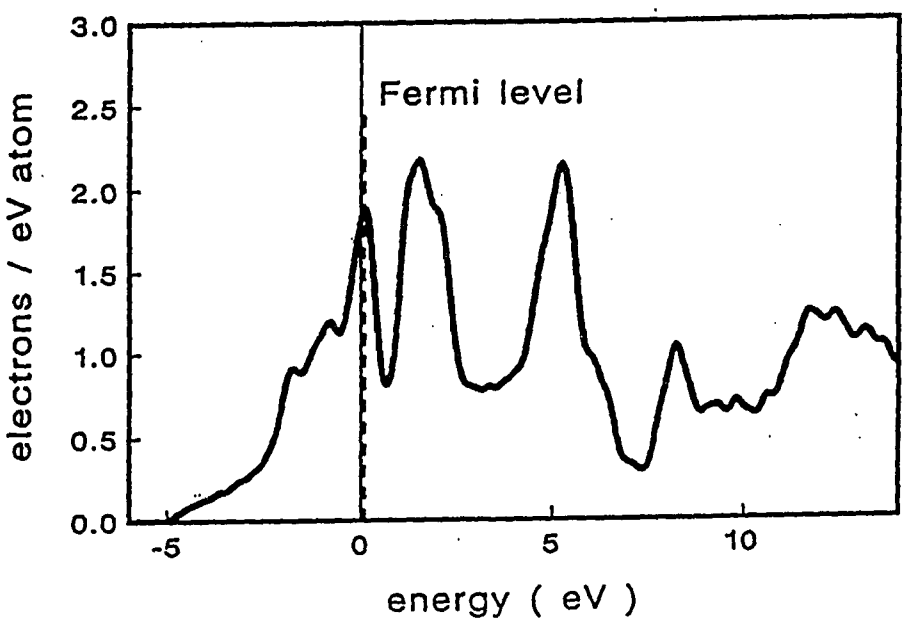

Figure 4.4: The density of states of hcp yttrium. The Fermi level is shown as the dotted line

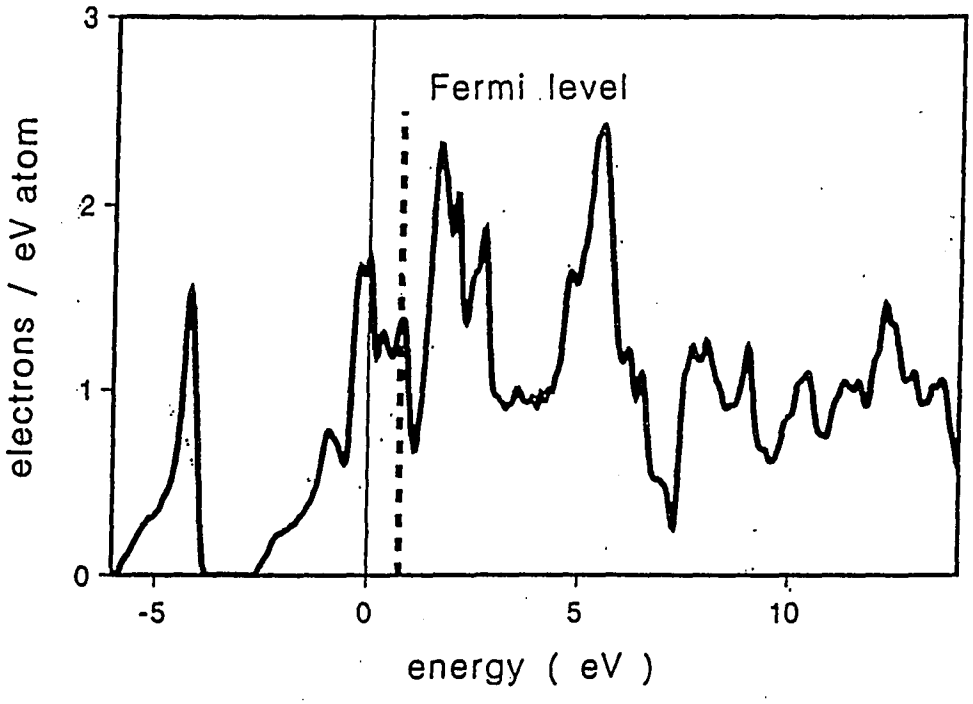

Figure 4.5: The density of states of $YH_{0.5}$. The Fermi level is shown as the dotted line

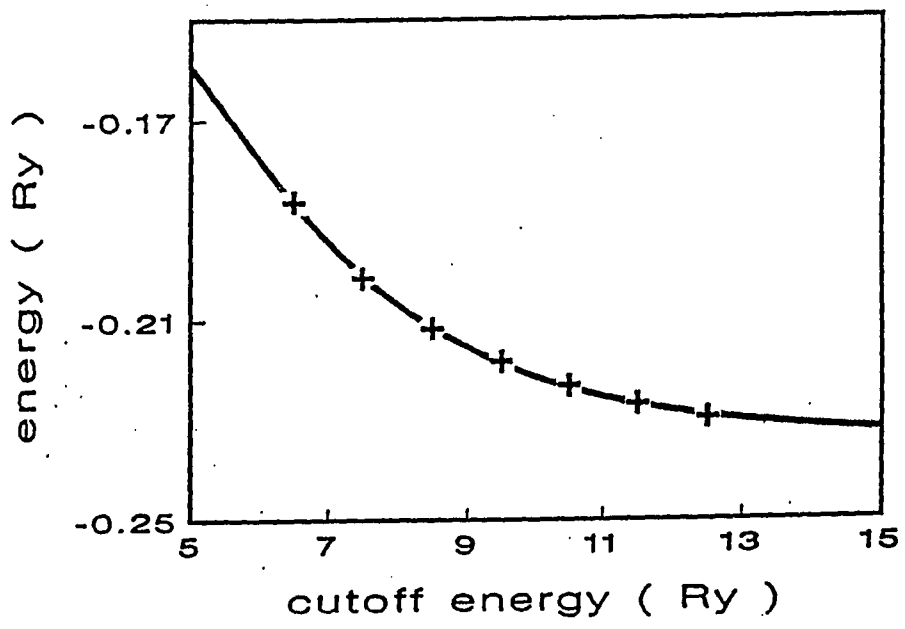

Figure 4.6: The convergence of the cohesive energy of $YH_{0.5}$ with respect to the bulk Y + atomic H as a function of the cutoff energy for the plane wave basis

CHAPTER 5. DYNAMIC PROPERTIES OF HYDROGEN IN α-$YH_{0.5}$

Introduction

Metal hydrogen systems exhibit a variety of interesting physical phenomena. Topics such as the ordering of the hydrogen in the host metal, the localized vibrations of hydrogen, and the transport of hydrogen through the lattice have been the subjects of many studies. The importance of the understanding of such phenomena in applications such as energy storage and the prevention of hydrogen embrittlement provides additional impetus to these investigations [1, 2, 3].

The behavior of hydrogen in hcp metals is distinguished from its behavior in the bcc and fcc metals by a number of unique features. A large amount of hydrogen can go into solid solution in the lattice at low temperatures without the precipitation of hydride phases [52]. Hydrogen remains in the disordered α-phase for a concentration up to 0.245 atomic ratio of H per Y atom and for a temperature range down to 4 K [52]. This extraordinary stability of the disordered phase at low temperature and relatively high concentration is fairly puzzling in view of the almost vanishing solubility in the bcc and fcc metals at low temperatures. The occurrence of pairing of the hydrogen atoms along the c-axis [53, 54, 60, 61] has also aroused much interest. A resistivity anomaly in the temperature range from 170 to 280 K [52] has been

observed in many hcp metals such as Lu [62] and Sc [63] and interpreted in terms of hydrogen pairing along the c-axis [53, 54, 60, 61]. The localized vibration frequency of H (D) atom in Y is noted for its unusual behavior. Assuming that the local vibration frequency of H in Y is decided mainly by the nearest neighbor atoms, the local symmetry of the tetrahedral(T) site (Figure 5.1) suggests threefold degenerate vibration frequencies for H (D). However, the inelastic neutron scattering measurement of the localized vibration of H (D) in α-$YH_{0.18}$ ($YD_{0.18}$) by I. S. Anderson *et al* [53, 54] reports nondegenerate vibration frequencies. We find that this signifies the importance of the strong anharmonicity of the hydrogen potential in determining the vibrational frequencies of the hydrogen atom along the c-axis. The long range diffusion of hydrogen has also been studied for a long time [4, 55, 57, 58, 59]. However, the potential energy surface of hydrogen in hcp metals has not been known in more detail. For example, confusion about the equilibrium interstitial site for hydrogen in hcp metals has led to wrong assumptions about the possible diffusion paths [64]. Strong isotope effects are also apparent in the low temperature thermal expansion of the lattice with dissolved hydrogen [65]. On the whole, we can say that, compared to bcc and fcc metals, the interactions of hydrogen with metal atoms in hcp metals have not been very well understood theoretically.

In this chapter, first principles total energy calculations are applied to study the localized vibrational states of hydrogen (H) and deuterium (D) in the α-phase YH_x (YD_x) system. First principles total energy calculations have been applied to various bcc and fcc metal-hydrogen systems [11, 12, 13, 14] with much success. Our own previous total energy calculation [15] of $YH_{0.5}$, with one H atom in the hcp primitive unit cell, has shown that the H (D) atom occupies the tetrahedral (T) site

of the hcp yttrium metal, in agreement with the neutron diffraction experiment of α-$YD_{0.18}$ by D. Khatamian et al [36]. Also the lattice expansion due to hydrogen and the heat of formation of $YH_{0.5}$ are in good agreement with the experiments [49, 51]. This provides a good background for a further study of dynamics of H (D) in α-YH_x via the first principles total energy calculation on $YH_{0.5}$.

There are some important factors in studying the dynamics of hydrogen in hcp metals. First, hydrogen is distinguished from the other interstitial atoms by its light mass. Thus quantum mechanical effects are important in the dynamical properties of the system at low temperatures. We map out the potential felt by the hydrogen atom in the metal lattice by calculating the total energy of the crystal as a function of the hydrogen position in the unit cell. We solve the Schrödinger equation for the vibrational states of hydrogen and its isotopes in the three dimensional potential obtained from the first principles calculations. We put one hydrogen atom in each hcp unit cell in our calculations. While this reduces the computational effort in the first principle calculations, it precludes the inclusion of lattice relaxation effects about the hydrogen atom other than by a uniform change in the lattice parameters. Further calculations with bigger unit cells and with lower hydrogen concentration are necessary to assess the effects of lattice relaxation as well as the effects of hydrogen-hydrogen interaction and pairing. The coupling of the hydrogen motion to lattice vibrations is another interesting problem difficult to include within the context of our present calculations. This is an area to be further explored in the future, possibly with tools such as molecular dynamics to include the effects of thermal motion of the lattice. First principles calculations could provide the necessary data base for fitting more empirical potentials for use in such studies. In spite of these imposed limitations

on our result, our calculation is able to provide new information and insight into the above mentioned problems.

Details of the Calculation

The total energy calculation proceeds in the same way as has been described in the previous chapter. Local orbitals of the form

$$f_{lm} = Nr^l exp(-\gamma r^s) Y_{lm}(\theta, \phi)$$

are used for Y, with $l = 1, s = 3, \gamma = 0.420$ a.u. for the 4p electrons and $l = 2, s = 2, \gamma = 0.90$ a.u. for 4d electrons. These are slightly different from what has been used in the previous study. One big difference, however, exists: a new hydrogen pseudopotential constructed according to the norm-conserving recipe is used for the study of dynamical properties. The norm-conserving hydrogen pseudopotential used in the present calculation differs from that used in previous calculations in that it has a smaller core radius of 0.7 a. u. to avoid problems with overlap core radii. This is important because the path from a T site to the facing T site, the path from a T site to the adjacent octahedral(O) site (Figure 5.1), and the direct path from an O site to the above O site are all passing through a bottleneck consisting of three Y atoms forming a triangle. A local orbital is included in our basis to help represent the hydrogen *1s* orbital. The local orbital is constructed to be the product of the hydrogen *1s* pseudowavefunction times a cutoff function of the form

$$f_{cut} = 1 - exp(-\alpha(r_c - r)^2), \tag{5.1}$$

where $r_c = 0.7$ a.u. is the cutoff radius and $\alpha = 4.40$ is used. The charge calculations are performed with a recently developed mixed basis charge symmetrization scheme

[66].

The total energy is calculated using the momentum space expression of the total energy per unit cell. The energy eigenvalues and the wave functions are sampled at 48 k-points inside the irreducible Brillouin zone(IBZ), and the Gaussian smearing method with Gaussian width 0.05 eV is used to accelerate the convergence of the total energy with respect to the number of k-points. Other details are same as in the previous chapter.

We proceed to study the vibrational properties of H in YH_x by considering $YH_{0.5}$. We repeat the calculation of the total energy of $YH_{0.5}$ unit cell, changing the position of the H atom inside the unit cell, and take the total energy per unit cell as the potential for the interstitial H atom. This describes the potential experienced by the hydrogen atom in the metal lattice in the presence of a rigid lattice. This corresponds to invoking the Born-Oppenheimer approximation for hydrogen motion in the lattice because of the big difference in the mass of the hydrogen atom and the mass of the metal atom.

Results and Discussion

Since we are using a new hydrogen pseudopotential with a smaller core, we have recalculated the equilibrium volume and c/a ratio of $YH_{0.5}$. The equilibrium volume decreases from 462 a. u. to 457 a. u. per hcp primitive unit cell, the bulk modulus also decreases from 0.55 M bar to 0.51 M bar. The c/a ratio is 1.62, which is the same as our previous calculation [15]. At this fixed c/a ratio, the total energy calculation is repeated for different locations of the H atom inside the unit cell. Fifteen points along the lines connecting the interstitial sites are considered (dotted lines in Figure 5.1).

Seven points on the line connecting a T site and the facing T site, five points on the line connecting an octahedral site (O site) and the facing O site, and five points in between a T site and the adjacent O site are taken.

The total energy as a function of hydrogen position is fitted to a periodic potential of the form

$$v(\mathbf{r}) = \sum_{\mathbf{G}} v(\mathbf{G}) exp(i\mathbf{G} \cdot \mathbf{r}). \tag{5.2}$$

Since the hydrogen-hydrogen distance remains unaltered in the displacement of the hydrogen atoms, we assume that the hydrogen-hydrogen interaction stays constant and can be ignored in the above fit. The Fourier coefficients of the metal-hydrogen pair potential $v(\mathbf{G})$ are determined by minimizing the least square error in the potential energy surface. The error in the fitting is less than 3 percent. Ten independent $v(\mathbf{G})$'s are taken in the fitting. The Fourier coefficients of the fitted pair potential is shown in Table 5.1. The fitted potential surface along the symmetry directions are shown with the first principles points in Figure 5.2 to Figure 5.4.

The Schrödinger equation is solved for the motion of the hydrogen atom in the three-dimensional potential given by Equation 5.2. The ground state energy level of the hydrogen is determined accurately to within 0.0007 meV. The uncertainties of the excited states considered are less than 0.005 meV. Approximately 25,000 plane waves are used for the expansion of the H wavefunction. Symmetry is utilized to reduce the size of the Hamiltonian to be diagonalized. However, the deuterium is more localized than the hydrogen and requires a larger basis set for convergence. Approximately 35,000 plane waves are used for the D wavefunction. The uncertainty in the ground state energy level of the deuterium is less than 0.0004 meV. These uncertainties are small enough to determine accurately the overlap integrals between the states located

at different interstitial positions.

The results are listed in Table 5.2 with their group representation and the oscillator quantum number (n_x, n_y, n_z) at either the T site or the O site. For higher quantum numbers, the states are not purely confined to the well at one site and it is no longer possible to identify each state with the oscillator quantum numbers located at individual interstitial sites. The zero point energy of H (D) atom is 190 (135) meV at the T site, and 108 (75) meV at the O site. This corresponds to the fact that there is more space around the O site than around the T site. The O site is higher in energy than the T site by 128 meV. This indicates that the H atom prefers a location where the screening charge is more available, thus lowering the energy. This is supported by experiment where the effective charge of hydrogen in yttrium is reported to be negative [55]. This is in direct contradiction to the belief that the hydrogen would be trapped in vacancies [64].

The potential along the c-axis about the T site is shown in Figure 5.2. It can be seen that the potential is indeed very anharmonic around the T site. Also when compared with the shape of the potential well along the TO direction, the potential is considerably softer along the c axis in the T-T direction. From the solution of the three-dimensional Schrödinger equation, the vibration frequency of the H (D) atom along the c axis is 100.6 (74.7) meV in excellent agreement with the observed value of 100.1 (75.8) meV. The vibration frequencies for H (D) atom perpendicular to the c axis are 127.7 (91.4) meV. The neutron inelastic scattering measurement [53] gives 134.2 (96.3) meV. As expected, the vibration frequency is significantly higher in the basal plane than along the c axis. The good agreement between our result and the inelastic neutron scattering experiment indicates that our approximations are indeed

valid as far as the local vibration is concerned.

There is a splitting in the energy levels of the H (D) atom, which is related to tunneling between two nearest neighbor T sites. The splitting in the ground state energy level will cause a peak to occur in the specific heat at a temperature corresponding to the magnitude of the splitting. There is no such experimental data for α-phase YH_x. However, in LuH_x [67], which is also a hcp metal, such a peak occurs at 0.1 K, which corresponds to about 0.008 meV. For ScH_x, the ground state splitting is about 0.37 k_B, or 0.031 meV [68]. We would expect a peak in the specific heat at about 0.6 K or slightly higher temperature for α-YH_x. For the $(0,0,1)_T$ state, the splitting is 4.1 meV in our calculation compared to about 5.0$\pm$0.5 meV from the inelastic neutron scattering experiment [69]. The magnitudes of the splittings of the energy levels are summarized in Table 5.3. The effect of the Born-Oppenheimer approximation of assuming a rigid lattice is two-fold: Correlation of the H motion with the motion of the lattice atoms would lower the potential barrier between the two facing T sites, since the Y-H interaction is repulsive. As the H atom moves towards the facing T site, the lattice atoms would move away from the H atom, opening up the triangular bottleneck and lowering the potential barrier. If we allow the c/a ratio of the lattice to relax fully for any hydrogen position, we find that the potential barrier is almost flattened out between the two T sites, increasing the splitting. However, inclusion of relaxation of the lattice around the hydrogen atom in the interstitial site would also increase the binding energy of the hydrogen atom at the equilibrium position and hence decrease the splitting. Since the Y-H distances are smaller at the bottleneck than at the T sites, the first effect is expected to be bigger than the second effect if the lattice is allowed to relax fully at each hydrogen

position. However, given that H is so light and moves much quicker than the metal atoms, the final result is difficult to estimate without furthermore involved studies. There is also the possiblity of coupling of conduction electrons to hydrogen, which is also reported to increase the proton "hopping" rates [70]. Such coupling would be important at a low temperature. Coupled with the quantum nature of the hydrogen, this poses a formidable problem at present. Since it is expected that such a process would have a strong dependence on the temperature, a quantum molecular dynamics simulation of hydrogen based on the first principles result may be needed for a study of this phenomena.

Tunneling also complicates the analysis of hydrogen diffusion problem in hcp metals. Since we do not have any splitting for the energy levels centered around the O site, there is practically no tunneling between a pair of O sites located along the c axis with a separation c/2. Thus the tunneling would be significant only between the pair of T sites separated by c/4. However, in the hcp lattice, the T sites occur in isolated pairs so that once the H atom has tunneled to the nearest neighbor T site there is no other opportunity for tunneling other than back to the original T site. So the tunneling motion described above contributes only to a local rattling of the H atom and not to any long range diffusion.

The possible long range diffusion path are shown in Figure 5.1. The path between the pair of T sites, between a T site and an adjacent O site, and the path between the pair of O sites separated by $c/2$ in the c-axis comprise the possible long range diffusion path. Since the O site has more space around it, it is very easy to assume that O-O path is very important in the long-range diffusion process. However, we find that the potential barrier height between a pair of O sites (850 meV) is significantly higher

than the potential barrier height between an O site and an adjacent T site(460 meV), making the direct O-O jump not plausible at low temperatures. This is consistent with the proposition from recent experiments that the interstitial site residence time for a jump from an O site to the above O site should be much larger than any other residence times [58, 59]. Thus only T-O jumps and T-T jumps are significant in the long range diffusion of hydrogen. This conclusion is supported by a recent report of isotropic diffusion coefficients by Gorsky effect measurements [71]. The nearly isotropic diffusion coefficient has been explained within the context of an atomistic jump model which ignores O-O jumps. For a jump from a T site to an O site, the activation energy is 460 meV, while for the reverse process, the activation energy is 332 meV from our calculation. The NMR measurement by L. Lichty *et al* [57] reports 510 meV as the activation energy for α-phase $YH_{0.2}$. Other experiments report 530 meV [58] and 570 meV [59] as the activation energy for α-phase $YH_{0.215}$. The local deformation around the hydrogen interstitial could increase the activation energy by a self-trapping mechanism [72].

The potential barrier between the T site and the O site is shown in Figure 5.3. As stated earlier, the O site is higher than the T site by 128 meV. If a simple classical Boltmann distribution is used to predict the occupation of an O site at temperature T, then taking account of 4 T sites and 2 O sites per primitive unit cell,

$$4f_T + 2f_O = 1 \tag{5.3}$$

$$f_O = f_T e^{-\Delta E/k_B T}, \tag{5.4}$$

where f_O and f_T are probability of occupation for a specific T or O site is occupied and ΔE =128 meV is the energy difference between the T and O sites. This would

lead to 0.3% of hydrogen occupying the O site at 300 K and 3.3 % at 573 K. If zero point energy is considered, $\Delta E = 46$ meV for H and $\Delta E = 68$ meV for D. Then, 3.2 % of D would occupy O site at T = 300 K and 10.8 % of D would occupy O site at 573 K. Experiments report that less than 5 % of D occupy O site at T = 300 K [36], about 10 % of D occupy O site at T = 573 K [73]. However, we have a large occupation of O site by H compared to experiment which reports that less than 3 % of H occupy O site at T = 873 K [60, 58]. Since the energy difference is not large, it would be important to include the local deformations around the H which would lower the T site energy by a self-trapping mechanism [72]. Higher O site occupations reported in earlier experiments are related to hydrogen trapping and can be reduced by annealing.

There is also an activation energy for a fast jump between two facing T sites. We have 162 meV for the activation energy between the T sites compared to 90 meV from quasielastic neutron scattering experiment [59]. Our value for the barrier height should represent the upper bound value and the deviation can be explained by the coupling between the hydrogen motion and the host metal lattice vibration. Again, a quantitative prediction cannot be made within the context of a first principles frozen phonon calculation and a quantum molecular dynamics study is due.

Summary

The potential energy surface for hydrogen in hcp yttrium metal is determined for the first time by first principles total energy calculations. The vibration frequencies of the hydrogen in α-phase YH_x have been calculated and are in excellent agreement with the experiment. The activation energy of the diffusion of the hydrogen also

agrees well with the experiments. From the splitting of the energy levels of H located at T site, a peak in the specific heat is predicted at a temperature slightly higher than 0.6 K. Since the present study is limited by the Born-Oppenheimer approximation between the H and Y atomic motions, a quantum molecular dynamics simulation would be needed for a better understanding of hydrogen diffusion in hcp metals. Since such simulations must include some empirical scheme in view of the present computing capacity, information from first principles total energy calculation will be useful for building such schemes.

Table 5.1: Fourier coefficients of the hydrogen-yttrium pair potential in mRy

G			V(G)
-1	0	0	109.2936
0	0	-2	93.9058
-1	0	-1	87.7994
-1	0	-2	35.1398
-2	1	0	14.7772
-1	0	-3	6.0114
-2	0	0	2.9116
-2	1	-2	4.1378
-2	0	-1	3.0328
0	0	-4	0.2758

Table 5.2: Energy level of the hydrogen and the deuterium in meV. (n_x, n_y, n_z) are the oscillator quantum numbers. Subscripts refer to the T site or the O site where the H (D) atom is located

(n_x, n_y, n_z)		H	D
$(0,0,0)_T$	Γ_1	189.83	134.54
	Γ_3	189.88	134.54
$(0,0,1)_T$	Γ_1	288.46	209.19
	Γ_3	292.56	209.37
$(1,0,0)_T$	Γ_5	317.58	225.99
	Γ_6	317.56	225.99
$(0,0,2)_T$	Γ_1	351.78	
	Γ_3	374.51	
$(0,0,0)_O$	Γ_1, Γ_3	235.58	203.38
$(0,0,1)_O$	Γ_2', Γ_4'	318.10	261.20
$(1,0,0)_O$	Γ_5', Γ_6'	304.52	251.06
$(0,0,2)_O$	Γ_1, Γ_3	374.51	
$(2,0,0)_O$	Γ_5, Γ_6	370.30	

Table 5.3: The splitting of the hydrogen energy levels centered at the T sites in meV

	H	D
J_{000}	0.053	0.001
J_{001}	4.103	0.183
J_{100}	0.015	0.001
J_{002}	33.519	6.078

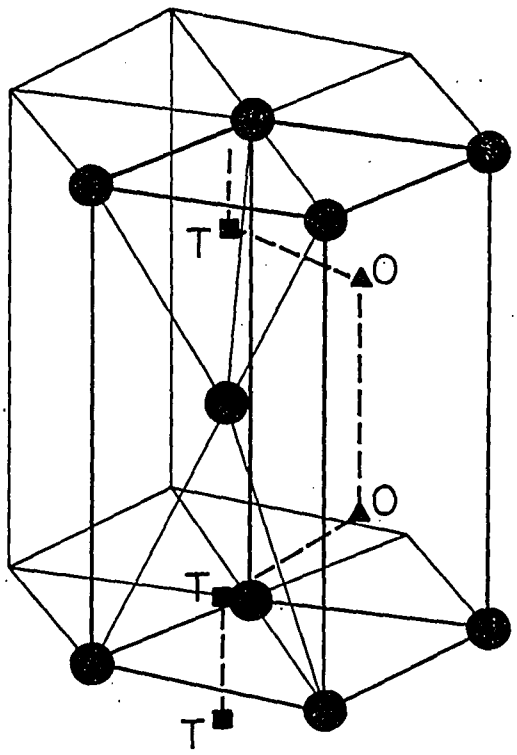

Figure 5.1: The $YH_{0.5}$ primitive unit cell. The total energy is calculated with the H atom located at symmetry directions connecting T-T-O-O sites

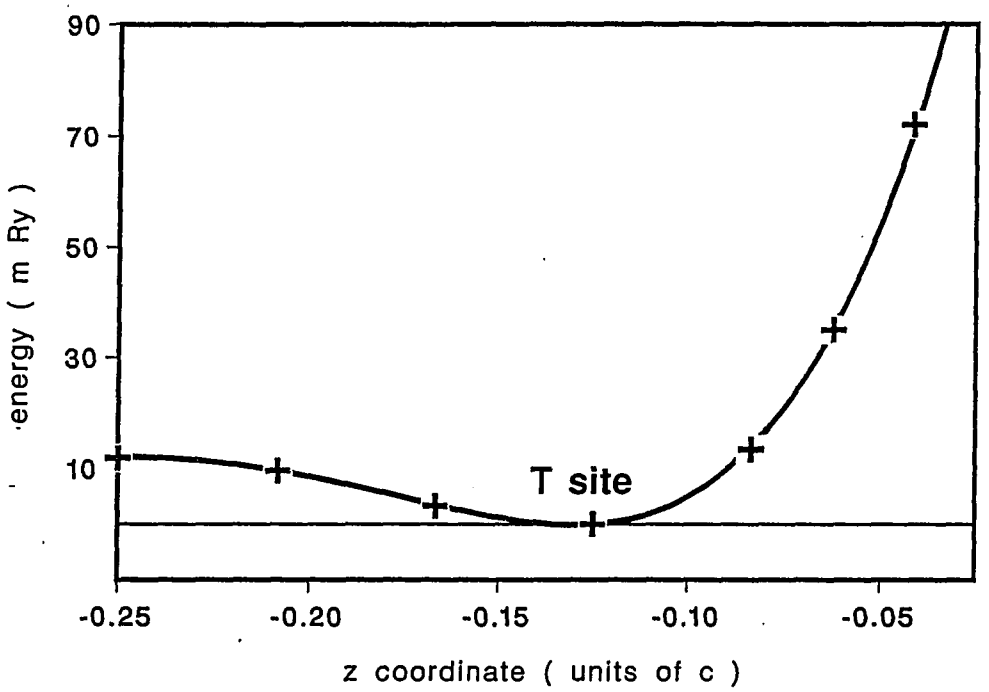

Figure 5.2: The fitted potential for H atom along the line connecting a T site and a facing T site, separated by $c/4$. The markers (+) represent the first principles total energy values

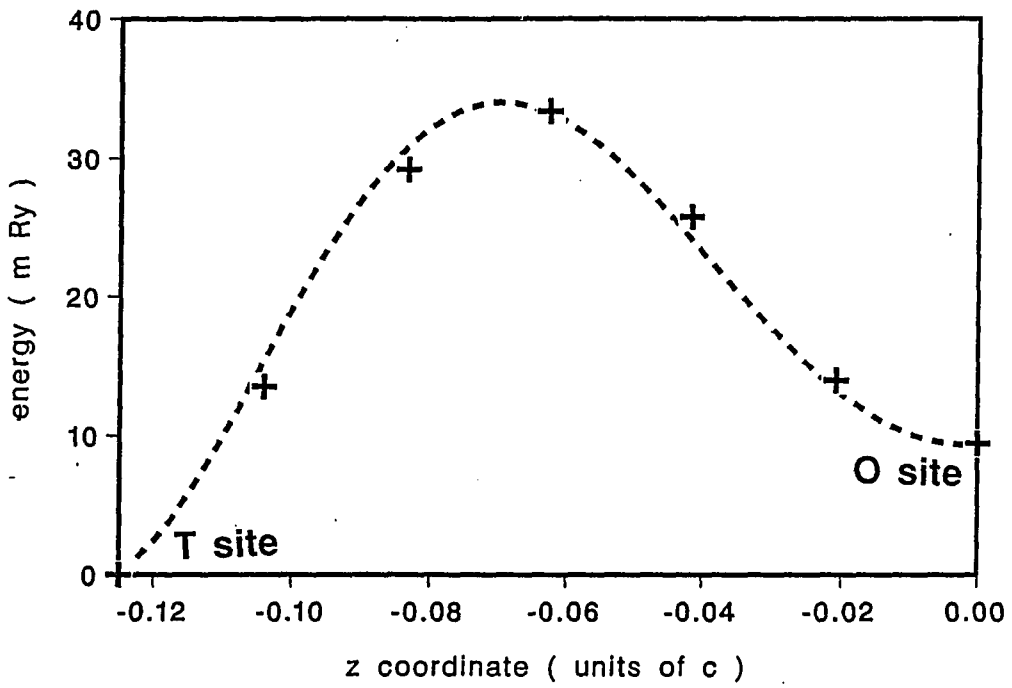

Figure 5.3: The fitted potential for H atom along the line connecting a T site and an adjacent O site. The markers (+) represent the first principles total energy values

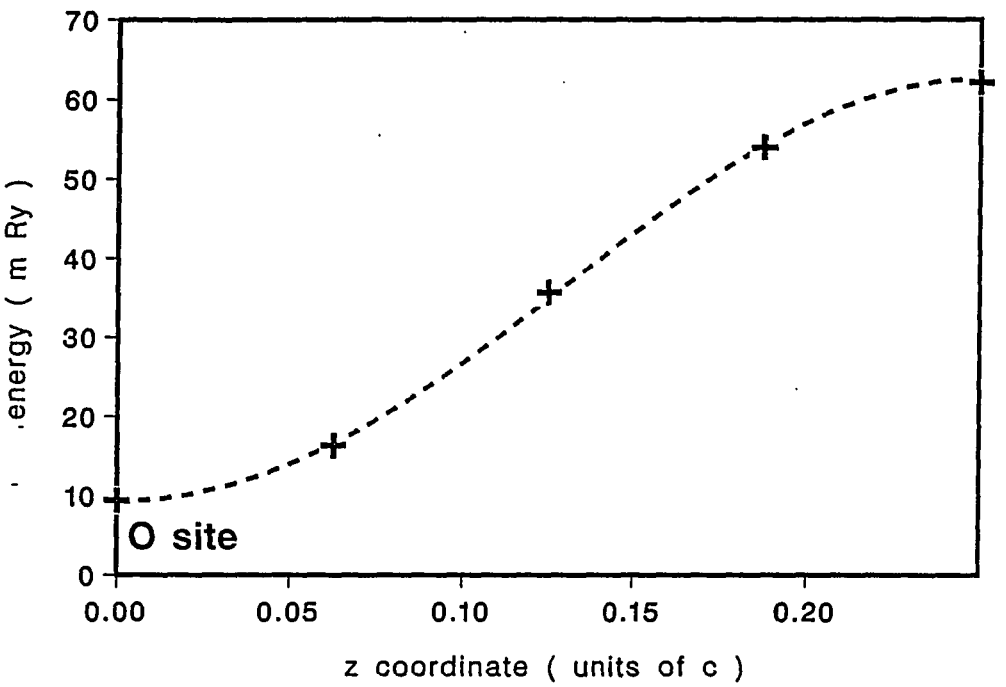

Figure 5.4: The fitted potential for H atom along the line connecting an O site and a facing O site, separated by $c/2$. The markers (+) represent the first principles total energy values

CHAPTER 6. EMPIRICAL TIGHT BINDING MOLECULAR DYNAMICS

Concept and Its Application to Silicon Hydrogen Systems

In view of the great success of the first principles total energy calculations, the logical next step is the study of dynamics under the same scheme. In such a context, Car and Parrinello [74] proposed a first principles molecular dynamics scheme using a fictitious Lagrangian method. However, its application is limited at present by the huge computational cost. This would also mean that a system with a complicated electronic structure, such as a transition metal system, cannot be treated at present. In addition, such a first principles scheme would be impractical as a candidate for a quantum mechanical treatment for hydrogen in the near future.

Since the pioneering work of Chadi [75], the empirical tight binding(ETB) model has been continually applied to studies of properties of semiconductors[76, 77, 78, 79, 80]. In these schemes, tight binding parameters are treated as parameters [101, 76] and determined by fitting to an accurate electronic band structure calculation. The tight binding scheme aims at modeling the variation of the total energy with atomic displacements via the incorporation of the basic features of the electronic band structure, which is described in terms of the minimal basis set of atomic orbitals. It is inevitable that the tight binding electronic band structure cannot be as accurate as

the first principles band structure, because of the basis set it employs. However, its computational cost is much less than the first principles calculation and can be useful for treating large systems where first principles calculations are not computationally feasible.

The success tight binding has had recently is quite impressive contrary to what is commonly believed to be the limits of the tight binding scheme. When applied to carbon, the phase diagram at zero temperature closely reproduces first principles results [82]. Also in the case of silicon, not only the phonon frequencies but also the mode Grüneisen parameters have been accurately reproduced to an accuracy comparable to that of the first principles calculation [83]. However, classical schemes [84, 85, 86, 87] have not enjoyed such an extensive success compared to the empirical tight binding scheme. Thus we are encouraged to apply the ETB scheme to a semiconductor hydrogen system with a view for a future application in a quantum mechanical simulation of hydrogen.

Silicon hydrogen systems have been studied for a long time for their importance in device technology and also for their array of interesting physical phenomena. Hydrogen is commonly used for passivating dangling bond defects in hydrogenated amorphous silicon systems [88] as well as in hydrofluoric acid etched crystalline silicon surfaces [89]. It has been found in experiments that the hydrogen causes changes in the electrical and optical properties, as well as the surface structures [90]. Nevertheless, the physical mechanism underlying these phenomena is still far from being completely understood. Due to the complexity of the systems, theoretical studies have been a great challenge. For example, in the first principles total energy calculation, we are aware that the surface relaxation of monohydride Si(111) surface is

sensitive to the hydrogen pseudopotential and the number of plane waves used in the calculation [91]. First principles calculations have produced some significant results [92, 93, 94, 95], but the computational cost is prohibitive for large systems. At this time, the maximum size of the system is about 100 atoms.

On the other hand, there are a few empirical classical interatomic potentials that has been proposed for hydrogen-silicon systems [96, 97]. These potentials have been used to build a computer model of amorphous silicon hydrides [96, 98]. Computational cost is not a problem here, but the reliability of the classical potentials in treating the dynamics of hydrogen-silicon systems is still an open question.

Several years ago, Allan and Mele extended the empirical tight binding scheme, which has been quite successful for pure silicon system[102], to the study of hydrogenated Si surfaces [103]. The advantage of the ETB model over the classical model is that the quantum mechanical bonding nature of the system is taken into account through the underlying electronic structure rather than through *ad hoc* N-body potentials [96, 97, 98, 84, 85, 86, 87]. The tight binding scheme is computationally efficient since it uses a minimal basis for the electronic calculations and the Hamiltonian matrix elements are parametrized. With the Chadi tight binding model[75] for silicon-silicon interactions a hydrogen-silicon interaction derived from the silane molecule,[103] Allan and Mele have produced some resonable results for the T=0 properties of the hydrogenated silicon surfaces. However, the tight binding model used by Allan and Mele has some drawbacks when considered for use in molecular dynamics simulations. Firstly, the symmetric and antisymmetric bending mode of silane(SiH_4) predicted by their model are about 30 % smaller than the experiment. Secondly, the model is constructed in the harmonic regime and is not adequate for

use in molecular dynamics simulations to study the properties of the system at high temperatures, where the anharmonic effects on the dynamics of hydrogens are very important. Furthermore, because of the large amplitude of the zero point motion of the hydrogen atom, anharmonic effects are not negligible even at very low temperatures.

We propose an improved tight binding model designed for use in molecular dynamics simulations of hydrogen-silicon systems. The hydrogen-silicon interaction is also derived from the silane(SiH_4) molecule proceeding in a similar way as Allan and Mele. However, our model includes anharmonic interactions and also reproduces accurately the vibration frequencies of the silane molecule. Further tests for the disilane molecule and for H on the Si(111) surface suggest that the model has very good transferability.

Empirical Tight Binding Scheme

The total energy of a system of electrons and ions is

$$H = T_e + T_i + V_{i-i}(\{R\}) + V_{e-e}(\{r\}) + V_{i-e}(\{r\},\{R\}),$$

where T_e is the electronic kinetic energy, T_i is the ionic kinetic energy, V_{i-i} is the ion-ion interaction energy, V_{e-e} is the electron-electron interaction energy, and V_{i-e} is the ion-electron interaction energy. {r} denotes the electronic coordinates and {R} the ionic coordinates. With the usual Born-Oppenheimer approximation between the electrons and the ions, the total energy is written as

$$E_{tot}(\{R\}) = V_{i-i}(\{R\}) + E_e(\{R\}),$$

where E_e is the total electronic energy which depends parametrically on the ionic configuration {R}. ETB attempts to express E_e in terms of the eigenvalues of the one-electron Hamiltonian

$$(T_e + V_{i-e} + V_{e-e})\psi_{n\mathbf{k}} = \varepsilon_{n\mathbf{k}}\psi_{n\mathbf{k}},$$

where n is the band index, and the k is the wave vector. Then

$$E_{bs} = \sum_{n\mathbf{k}} \varepsilon_{n\mathbf{k}} f_{n\mathbf{k}},$$

where $f_{n\mathbf{k}}$ is the Fermi function. E_{bs} is the band structure energy calculated as the sum of occupied electronic eigenvalues. In obtaining $\varepsilon_{n\mathbf{k}}$, the two-body electron-electron interaction terms have been included as a one-body effective potential. Therefore E_{bs} includes the electron-electron interaction twice, and this double counting should be corrected.

We can define

$$U_0(\{R\}) = V_{i-i}(\{R\}) - < V_{e-e}(\{R\}) >,$$

where <> denotes the expectation value. This arrangement of the terms has the advantage that for two ions that are separated by a distance much larger than the Thomas-Fermi screening length the combined effect of the ion and the screening electron system is nearly neutral, making $U_0(\{R\})$ zero. Thus $U_0(\{R\})$ is a short ranged repulsive potential. Now the total energy is written as

$$E_{tot}(\{R\}) = U_0(\{R\}) + E_{bs}(\{R\}),$$

where

$$U_0(\{R\}) = \sum_{<i,j>} \phi_{i,j}$$

is the two-body potential energy calculated from a two-body potential ϕ. $U_0(\{R\})$ is determined by subtracting E_{bs} from the E_{tot} provided the latter is known either from first-principles total energy calculations or from experiments. In a molecular dynamics simulation, atoms will be subject to two kinds of forces, the Hellmann-Feynman force arising from the band structure term

$$\mathbf{F}_i^{HF} = -\sum_{n\mathbf{k}} f_{n\mathbf{k}} < \psi_{n\mathbf{k}} | \frac{\partial H}{\partial \mathbf{R}_i} | \psi_{n\mathbf{k}} >$$

and the two-body force from the two-body potential

$$\mathbf{F}_i^{two-body} = -\frac{\partial}{\partial \mathbf{R}_i} U_0(\{R\}),$$

where H is the tight binding Hamiltonian.

Molecular Dynamics

Since the introduction of the electronic computers, a great amount of effort has been made in the pursuit of a realistic molecular dynamics. Especially its powerful capacity in the study of temperature dependent phenomena has provided an exciting new possibility.

Molecular dynamics(MD) is a technique to calculate statistical ensemble averages of classical interacting many-body systems. MD studies the equilibrium and nonequilibrium thermodynamic systems by sampling a sequence of configurations connected by the coupled Newton's equation

$$m_i \frac{d^2 \mathbf{r}(t)}{dt^2} = -\mathbf{F}_i. \tag{6.1}$$

The output trajectories $(\mathbf{r}(t), \mathbf{p}(t))$ then provide information about the statistical properties of the system. This set of coupled differential equations (Equation 6.1)

is solved via finite difference approach [99, 100]. Given the molecular positions, velocities, forces, and other dynamic information at time t, attempts are made to determine the positions, velocities, etc. at a later time $t + \delta t$ to a sufficient degree of accuracy. The equations are solved as an intial value problem, and the choice of δt should be much smaller than its characteristic times, such as the phonon vibration period.

We have used Gear's 6-th order predictor-corrector algorithm. Assuming the classical trajectory is continuous, an estimate of the positions, velocities, etc. at time $t + \delta t$ is obtained by Taylor expansion about time t:

$$\frac{d^n}{dt^n}\mathbf{r}^P(t+\delta t) = \sum_{k=0}^{5-n} \frac{\delta t^k}{k!}\frac{d^k}{dt^k}\mathbf{r}(t), n = 0, 1, 2, ..., 5 \tag{6.2}$$

where $\mathbf{r}$ stand for the complete set of positions, and the superscript P means that these are the predicted values. The above Equation 6.2 will not generate correct trajectories as time advances, because the equations of motion have not been introduced yet. The correct forces at time $t + \delta t$ are calculated from the new predicted positions $\mathbf{r}^P$, and hence the temporary accelerations $\frac{d^2}{dt^2}\mathbf{r}^T(t+\delta t)$. These are then compared with the predicted acclerations from Equation 6.2 to calculate the force correction parameter via

$$\Delta F = \frac{1}{2}\delta t^2[\frac{d^2}{dt^2}\mathbf{r}^T(t+\delta t) - \frac{d^2}{dt^2}\mathbf{r}^P(t+\delta t)].$$

The predicted parameters computed in Equation 6.2 are now corrected with the Gear coefficients G_i via

$$\frac{d^n}{dt^n}\mathbf{r}^C(t+\delta t) = \frac{d^n}{dt^n}\mathbf{r}^P(t+\delta t) + \frac{n!}{\delta t^n}G_n\Delta F, n = 0, 1, 2, ..., 5$$
$$G_0 = \frac{3}{16}, G_1 = \frac{251}{360}, G_2 = 1, G_3 = \frac{11}{18}, G_4 = \frac{1}{6}, G_5 = \frac{1}{60}.$$

The superscript C denotes the corrected positions. These new corrected values are now taken as the current position, velocity, etc., and all analyses at this time step are performed using these values. This entire procedure is then iterated for the duration of the simulation. Although, in principle, this corrector step may be iterated to further refine the trajectory, it is commonly not used since the force calculation is expensive.

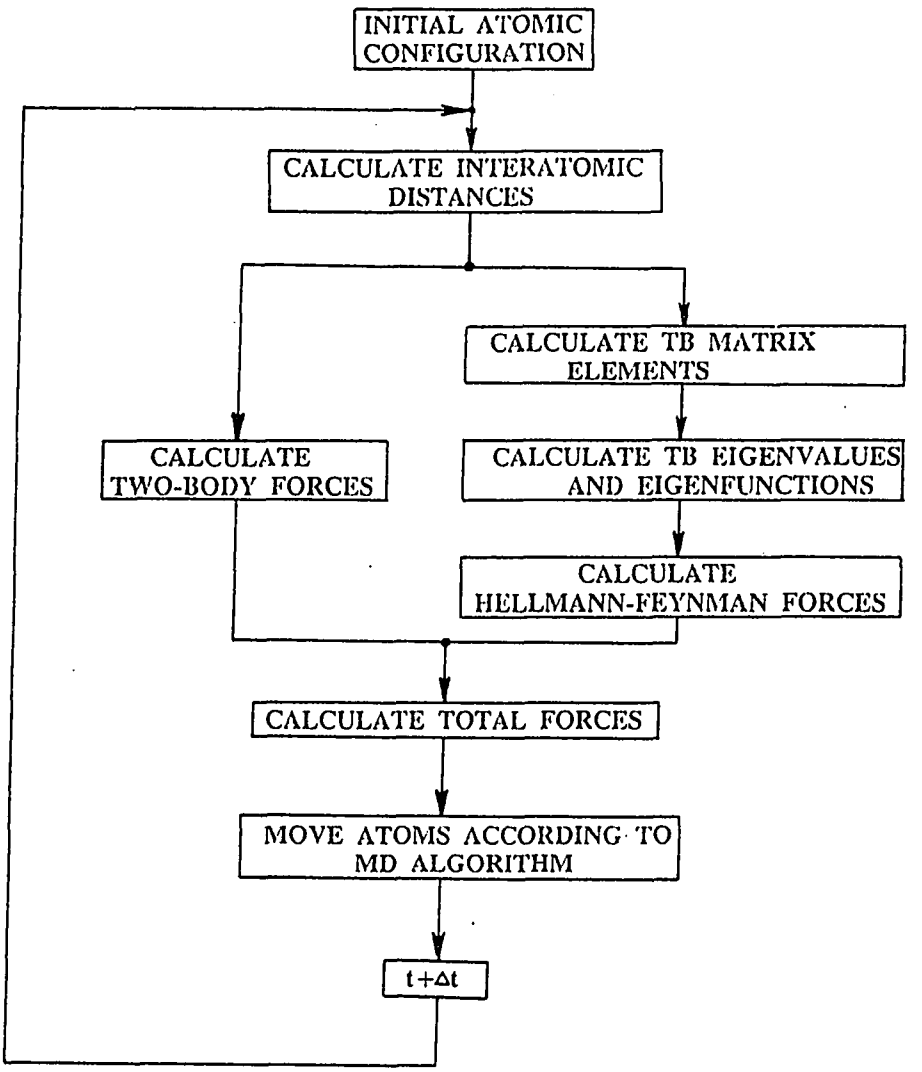

Figure 6.1: An illustration of empirical tight binding molecular dynamics(ETBMD) routine

CHAPTER 7. EMPIRICAL TIGHT BINDING MODEL FOR THE SILICON HYDROGEN SYSTEM

Silicon-Silicon Interaction

The Si-Si ETB model is taken from C. Z. Wang, C. T. Chan, and K. M. Ho [83]. The tight binding parameters for the description of the electronic structure are taken from Chadi's previous work on the empirical orthogonal tight binding model for Si [75]. The electronic states are represented by an orthogonal basis containing four sp^3 orbitals per Si atom. The two-center approximation [101] is used for the calculation of the interatomic matrix elements and only nearest neighbor interactions are taken into acount. The tight binding parameters are determined by fitting to the calculated band structure of Si in the diamond structure. The tight binding parameters are as follows (in eV):

$$V_{ss\sigma}(d_0) = -1.94 \quad , \quad V_{sp\sigma}(d_0) = 1.75,$$
$$V_{pp\sigma}(d_0) = 3.05 \quad , \quad V_{pp\pi}(d_0) = -1.08,$$
$$E_s = -5.20 \quad , \quad E_p = 1.20,$$

where d_0 is the $T = 0$ equilibrium nearest neighbor distance. The bond length dependence of the two-center parameters is assumed to follow Harrison's universal

r^{-2} scaling behavior [76],

$$V_{ss\sigma}(r) = V_{ss\sigma}(d_0)(d_0/r)^2,$$
$$V_{sp\sigma}(r) = V_{sp\sigma}(d_0)(d_0/r)^2,$$
$$V_{pp\sigma}(r) = V_{pp\sigma}(d_0)(d_0/r)^2,$$
$$V_{pp\pi}(r) = V_{pp\pi}(d_0)(d_0/r)^2.$$

Unlike the original Chadi model, which fit the two-body potential to the lattice constant and the bulk modulus of Si, Wang *et al* derive the two-body potential energy function $U(r)$ by subtracting the ETB band structure energy function $E_{bs}(r)$ from the first-principles total energy function $E_{tot}(r)$, i.e.,

$$U(r) = E_{tot}(r) - E_{bs}(r),$$

where r is the nearest neighbor distance of the diamond structure. The total energy function $E_{tot}(r)$ is taken from the results of Yin and Cohen [8] and fitted to the universal binding curve [43]

$$E_{tot}(r) = E_0(1+x)e^{-x}, x = \frac{r-r_0}{A}$$

with E_0=-4.8060 eV, $r_0 = 2.3627\mathring{A}$, and $A = 0.5076\mathring{A}$. The ETB results of E_{bs} are also fitted to a third order polynomial

$$E_{bs}(r) = A_0 + A_1(r-r_b) + A_2(r-r_b)^2 + A_3(r-r_b)^3$$

with $A_0 = -23.37$ eV, $A_1 = 17.32$ eV/$\mathring{A}$, $A_2 = -12.42$ eV/$\mathring{A}^2$, and $A_3 = 5.25$ eV/$\mathring{A}^3$.

By further assuming that the two-body potential contains only the nearest neighbor interactions and each nearest neighbor contributes equally to the total two-body potential energy, we can extract the pair potential for the molecular dynamics simulation

$$\phi(r) = \frac{1}{2}[E_{tot}(r) - E_{bs}(r)]$$

which can be expressed in an analytic form via the analytic forms of $E_{tot}(r)$ and $E_{bs}(r)$. Molecular dynamics studies using this potential have produced a quantitative description of the temperature dependent frequency shifts and phonon linewidths of the phonons in crystalline Si [83]. The success of this empirical tight binding model in studying the anharmonic properties of Si could be attributed to the incorporation of detailed accurate total energy information.

Silicon-Hydrogen Interaction

The Si-H tight binding parameters are fit to the occupied eigenvalues and the symmetric bending mode vibration frequency of the silane(SiH_4) molecule, proceeding in a similar way as Allan and Mele [103]. We obtain (in eV)

$$E_s = -8.0, V_{ss\sigma} = -3.63, V_{sp\sigma} = 4.63.$$

Again, the bond length dependence of the hopping parameters is assumed to follow the $1/r^2$ scaling law [76]. Unlike the previous work of Allan and Mele [103], we do not require the model to reproduce the eigenvalues of the antibonding states in silane. We believe that the eigenvalues of the empty states are not well described with a minimal basis set for Si.. This is consistent with the fact that the Chadi model gives

a poor description of the conduction bands in crystalline Si. Thus we obtain results which are higher than the experimental values. We think the further improvement of the basis set by including extra orbitals for Si will bring the empty states lower towards the experimental value. However, since the antibonding states are far away from the Fermi level, this will not strongly affect the energetics of the system. We find that $V_{sp\sigma}$ is now much larger than Allan and Mele's, providing more realistic bond bending forces. This improvement will be important for the bond bending modes where only the tight binding term is contributing to the restoring force.

The universal binding curve [43] is used to parametrize the total energy per bond E_{tot} of the silane(SiH_4) molecule as a function of Si-H bond length r_H:

$$E_{tot} = -E_H(1+x)e^{-x}, x = (r_H - d_H)/l_s$$

where $E_H = 3.355$ eV and $d_H = 1.48$ $\AA$ are the experimental values of bond energy [104] and equilibrium bond length of silane, and the scaling length $l_s = 0.4264$ $\AA$ is fitted to the vibration frequency (271.4 meV) of the symmetric stretching mode of silane with the procedure which will be described in next paragraph. The repulsive potential between the hydrogen-silicon pair is then determined by subtracting the bond-length dependence of E_{bs} of silane from the above universal binding curve. The significance of this formulation is that anharmonic information is included in the two-body repulsive potential as well as the tight binding term. This is essential for use in a molecular dynamics simulation. Since Allan and Mele make the expansion of the two body repulsive potential only up to the second order, their model is not adequate for a molecular dynamics simulation.

There is one minor technical difference between the Si-Si two-body potential construction. Since hydrogen mass is light, it is expected that the hydrogen displace-

ments will be unusually large. Thus it is important that the two-body potential be defined for a rather wide range of bond length r_H. We take the range between 1.184 $\AA$ and 1.776 $\AA$. Because of this reason, a cubic spline interpolation scheme is used for an expression of the two-body potential. Computationally, the two-body potential is still calculated in a polynomial form, only the interval where the bond length belongs to has to be selected before the calculation. The additional computational cost is marginal with this scheme.

Due to the light mass of the hydrogen atom, we find that it is important to include the zero point motion of the hydrogen atom in our molecular dynamics simulation to obtain an accurate description of the experimental phonon frequency shifts and phonon linewidths for the hydrogen vibration. Because of the large amplitude of the hydrogen zero point motion, we have found that the frequency of the stretching mode frequency of silane obtained from the molecular dynamics simulation at low temperature is shifted to lower frequency by about 5 meV compared to that obtained by frozen phonon calculations performed with small displacements. Since we want to use our model in a molecular dynamics simulation, we choose to include the large vibration amplitude of hydrogen at the earliest stage in the fitting of the stretching mode of hydrogen in silane for consistency. For fitting the parameter l_s, simulation is performed for a hydrogen atom moving in a potential well given by the universal binding curve, with an initial distortion amplitude estimated from the zero point energy of hydrogen in the given well. The parameter l_s is adjusted such that the frequency of the hydrogen obtained from the molecular dynamics simulation is equal to 271.4 meV. For comparison, the frozen phonon calculation with a small displacement would give 276.5 meV which would be 5 meV higher than the experimental value.

The hydrogen-hydrogen interaction is neglected for the present. This approximation is adequate for systems where the H-H interatomic distances are large (for example, the monohydride phase on Si(111) where H-H distance is 3.84 Å). H-H interaction may be needed for systems where the hydrogen atoms are much closer to each other, for example, in cases where dihydride and trihydride phases exist.

Results and Discussion

Results of the energy levels and vibrational frequencies for the silane(SiH_4) molecule calculated by the above tight-binding model are listed in Table 7.1 in comparison with experimental data and the previous tight-binding calculation of Allan and Mele [103]. The eigenvalues of the bonding states (a_1^+ and t_2^+) agree very well with the experiment, while the eigenvalues of the antibonding states (t_2^- and a_1^-) are higher than the experimental values. We attribute the poor results for the antibonding states to the use of only sp^3 orbitals for silicon atoms. If one includes also d orbitals to represent the electronic states of silicon atoms, the antibonding energy levels would be lower than the present values. Judging from past experience with silicon and carbon systems, an accurate description of the bonding states should be sufficient for studying the structural properties of the system. This becomes clear if we compare the bending mode frequencies of the silane(SiH_4) molecule with the experimental value. Since the bending mode frequencies are decided solely by the TB parameters and not related to the two-body potential, they are directly related to the quality of the TB parameters. The symmetric bending mode is in excellent agreement with experiment while the asymmetric bending mode is about 10 % less than the experimental value. The results suggest that our present tight-binding pa-

rameters are more suited for studying the vibrational properties of hydrogen-silicon systems than those in the previous work by Allan and Mele [103]. Results for the disilane(Si_2H_6) molecule are summarized in Table 7.2 with the experimental vibration frequencies[105].

Having established the model, we proceed to calculate the electronic properties, surface relaxations and the phonon vibration frequencies of the hydrogenated Si(111) surface. We have chosen a slab in the (111) direction which has 12 Si layers in the case of monohydride surface. Two hydrogen layers are added on top and bottom of the slab (Figure 7.1). We have used 120 and 55 k-points respectively in the irreducible part of the first Brillouin zone to calculate the surface electronic density of state and band-structure energy E_{bs}. The convergence of the above **k**-point samplings have been verified to be enough, for both the clean Si(111) surface and the monohydride surface.

Shown in Figure 7.2 is the local electronic density of states(LDOS) for the Si(111) monohydride surface. The arrows indicate the prominent hydrogen-related peaks. The LDOS's have a characteristic three-peak feature below the Fermi energy, with the peak at the lowest, medium and highest energy having s-like, s-p like and p-like characters respectively. It compares quite well with the results from more accurate self consistent calculations [106].

Results of surface relaxation of the monohydride Si(111) surface are presented and compared with first-principles calculation results in Table 7.3. In our calculations, the hydrogen layer and two outermost Si layers are allowed to relax in the (111) direction only. For the monohydride Si(111) surface, the present tight-binding model predicts slightly outward relaxation of the top layer of silicon, in contrast with

the first-principles calculation result which shows slight contraction. The equilibrium bond length between hydrogen and silicon of the monohydride phase is 1.49 $\AA$ from the tight-binding calculation which is smaller than the first-principles result of 1.54 $\AA$ [94].

Finally, the vibration frequencies of hydrogen on the monohydride Si(111) surface are presented in Table 7.4. The frequencies of the stretching and wagging modes predicted by the present tight-binding model are in excellent agreement with experimental data and first-principles calculation results. For the trihydride Si(111) surface, the symmetric bending mode frequency 93 meV is about 15% lower than the experimental value 108 meV. Since in the trihydride phase, the distance between the hydrogen pair is smaller (about 2.2 $\AA$), the neglect of the H-H interactions may cause the underestimation for the bending mode frequencies.

Summary

We have established an empirical tight binding model for the study of silicon hydrogen system. Our model gives good results for the hydrogenated Si(111) surface. In particular, the vibrational frequencies of the hydrogen are reproduced in a satisfactory way. The simplicity of the model makes it applicable for study in a problem where large systems have to be considered, such as for surface problems and amorphous silicon.

Table 7.1: Comparison of calculated SiH_4 eigenvalues in eV and bending mode frequencies in meV with experiment and other theoretical calculations

mode	experiment	Allan and Mele [103]	present work
a_1^-	-4.10	-5.17	-2.84
t_2^-	-5.40	-4.95	-1.93
t_2^+	-12.70	-12.59	-12.71
a_1^+	-18.20	-18.82	-18.23
symmetric bending	121	71.7	122
antisymmetric bending	113	72.6	103

Table 7.2: Comparison of calculated Si_2H_6 eigenvalues (in eV) and frozen phonon calculation results of hydrogen vibration frequencies in the disilane molecule (in meV). With the consideration of the zero point energy, the stretching mode frequency should get lower by about 5 meV.

mode	experiment	Allan and Mele [103]	present work
a_g	-10.7	-10.93	-11.07
e_g	-12.1	-12.38	-12.28
e_u	-13.3	-12.85	-13.23
a_u	-17.3	-17.27	-16.65
a_g		-19.18	-18.71
stretching	248		276
wagging	78		75
twist	62		55

Table 7.3: Surface relaxations of the monohydride Si(111) surface compared with first principles calculation result. "Ideal" corresponds to the case without any surface relaxations. All lengths are in $\AA$. Interplanar spacings d_H, d_1, and d_2 are defined in Figure 7.1. We take the bond length between Si and H in the silane(SiH_4) molecule as the sum of covalent radii of Si and H

	present calculation	first principles calculation [94]	ideal
d_H	1.49	1.54	1.48
d_1	0.81	0.72	0.78
d_2	2.35	2.32	2.35
d_1,clean	0.79	0.57	0.78
d_2,clean	2.39	-	2.35

Table 7.4: Hydrogen vibration frequencies on the monohydride Si(111) surface in meV. Our empirical tight binding result for the stretching mode includes the zero point motion of hydrogen. The first principles calculation is a small amplitude calculation in which case the frequency would get lower upon consideration of zero point motion of hydrogen

	present calculation	first principles calculation [94]	experiment
stretching	270	245	257
wagging	74	71	77

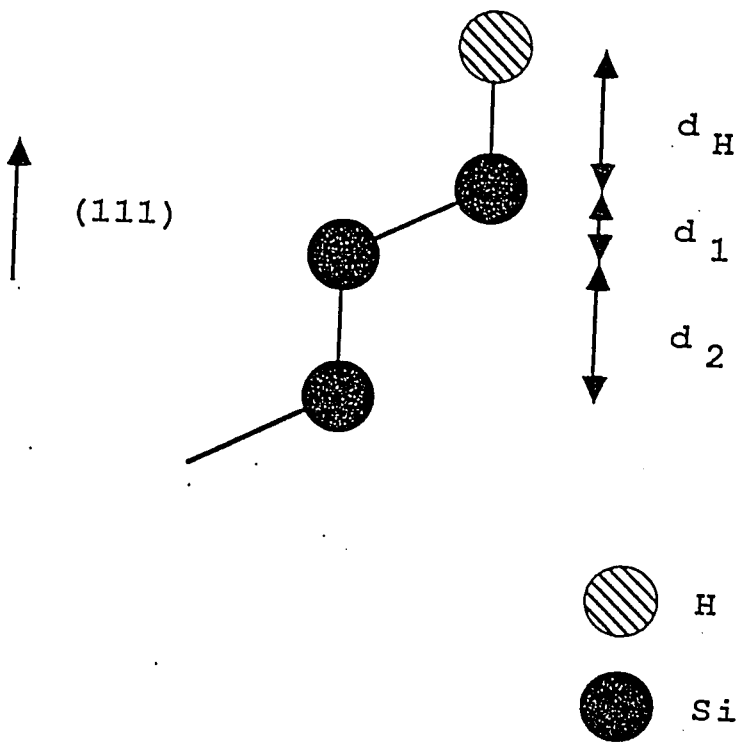

Figure 7.1: Surface geometry of the monohydride Si(111) surface

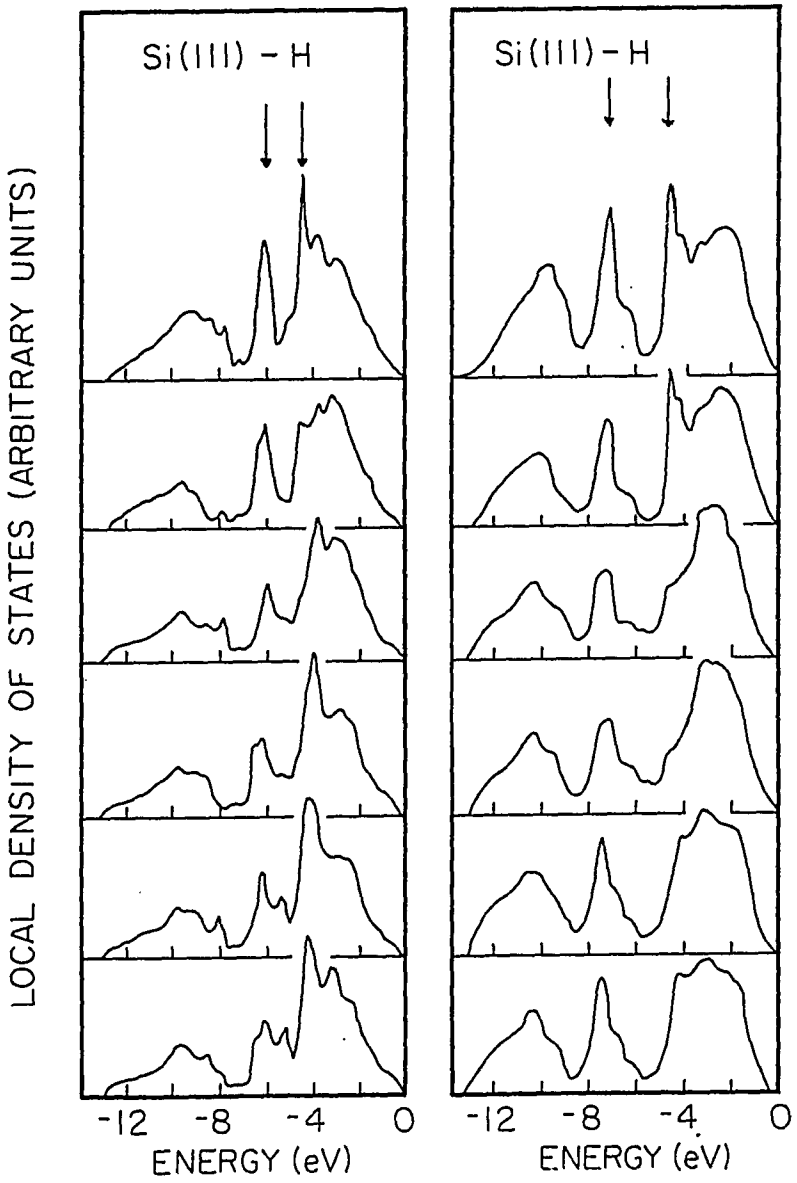

Figure 7.2: Local electronic density of states for the monohydride Si (111) surface from the present ETB calculation(left) compared with the first principles result (right). The top row figure corresponds to the hydrogen layer and the outermost Si layer. The second row figure corresponds to the second Si layer, and so on

CHAPTER 8. MOLECULAR DYNAMICS SIMULATION OF HYDROGEN VIBRATION ON THE Si(111) SURFACE

Introduction

Vibration frequencies of hydrogen on silicon surfaces have been commonly assigned to the characteristic modes of silicon hydrides (e.g. SiH, SiH_2 or SiH_3) [107]. Using high resolution electron energy loss spectroscopy (HREELS), however, H. Fröitzheim, H. Lammering, and H.-L. Günter [108] have shown that for a Si(111):H system, an extra loss at 62 meV is found in addition to losses that correspond to the hydrogen stretching mode (259 meV) and wagging mode (79 meV) of SiH. Similar phenomena have been also observed for Si(111):D [109] and Si(100):H [110] systems. Froitzheim *et al* [108] speculated that this extra loss is due to a substrate mode induced by the adsorbate and possibly coupled to the bulk phonons of Si [109]. Such considerations are supported by an empirical lattice dynamical model [111] based on a bond charge model [112], where the force constants related to the hydrogen stretching and bending modes on the surface are fitted. However, in a recent first-principles local density functional calculation of the vibrational properties of hydrogen on Si(111) and Ge(111) surfaces by E. Kaxiras and J. D. Joannopoulos [94], no attention has been paid to the extra EELS loss. Thus, at this time, there is no theoretical explanation for the phenomena at the microscopic level. Since the existence of the extra

mode on the adsorbate layer appears to be an intrinsic property of the hydrogen on Si adsorption system, knowledge about the nature of this extra mode could be crucial for better understanding of the interatomic interactions in chemisorption systems.

Modern surface preparation techniques have made it possible to fabricate a clean Si(111)(1×1):H surface [89] and to provide detailed experimental data with much reduced noise. The vibrational frequency of hydrogen on the Si(111) surface and related anharmonic effect, such as frequency shift and intensity loss, have been extensively measured [113]. However, microscopic mechanisms are not well understood.

We have performed a lattice dynamical calculation and a molecular dynamics(MD) simulation of vibrational behavior of a Si(111):H system to address these problems. Our results show that the origin of the extra EELS loss at 62 meV can be explained by coupling between the SiH wagging mode and a Si substrate phonon mode.

Results and Discussion

Using the empirical tight-binding model described in the previous chapter, a lattice dynamical calculation and an MD simulation is performed for a Si(111):H slab consisting of 6 layers of Si and two layers of H (attaching to dangling bonds on each Si(111) surface) and with nine atoms on each layer. In-plane periodic boundary conditions are imposed. This size is found satisfactory by comparing the results with that from a thicker slab (10 layers of Si) or a larger in-plane unit cell (16 atoms each layer).

In the lattice dynamical calculation, the force constant matrix K is determined by calculating the forces F on each atom for small displacements x of each atom in

the 6 layer unit cell,

$$F_{i\alpha} = -\sum_{\beta} K_{i\alpha,j\beta}\, x_{j\beta},\ i,j = 1,2,...N,\ \alpha,\beta = 1,2,3. \tag{8.1}$$

Then the normal modes of the system are determined by

$$det(K_{i\alpha,j\beta}\, x_{j\beta} - M_i\omega^2 x_{i\alpha}) = 0. \tag{8.2}$$

We consider a 6 layer unit cell with the k-point sampling equivalent to the $3 \times 3 \times 6$ MD cell to calculate the Hellmann-Feynman force arising from the band structure energy.

In the MD simulation, the phonon spectrum is obtained by taking the Fourier transform of the velocity-velocity autocorrelation function.

$$G(\vec{k},\omega) = \int dt e^{i\omega t} \sum_{n} e^{-i\vec{k}\cdot\vec{R}_n} \frac{<\vec{v}_n(t)\cdot\vec{v}_0(0)>}{<\vec{v}_n(0)\cdot\vec{v}_0(0)>}. \tag{8.3}$$

In this formulation, the phonon spectrum for each layer of the slab can be verified by taking the velocities of the particles that belong to specific layers only. Since the stretching mode of H is well separated from any other phonon modes in frequency and does not exchange energy with other modes, it is possible to simulate the effect of large zero point motion by depositing an energy equivalent to the zero point energy of the stretching mode in each Si-H bond. The simulation is performed at temperature ranges from 200 K to 600 K. At each temperature, the system is allowed to equilibrate for more than 10,000 MD steps. The time step Δt is taken as 2.7055×10^{-16} sec. After the equilibration of the system, 65,536 MD steps(corresponding to total time interval of 1.77×10^{-11} sec) are collected for the analysis.

In Figure 8.1, the oscillator strength at each layer, which is just the magnitude of the normal mode at the specific layer from the lattice dynamical calculation, is

plotted against the normal mode frequency for Si(111):H in Figure 8.1. Three major peaks appears in the H layer in Figure 8.1, at 62, 78, and 275 meV.

In Figure 8.2 , our results for the phonon spectrum of the hydrogen overlayer (on top) and the silicon substrate layers at 300° K (MD temperature) are presented. We see that on the hydrogen overlayer, three strong peaks have been observed at positions of 267 meV, 77 meV, and 61 meV, which are consistent with the lattice dynamical calculation results. The first two modes are strongly localized on the hydrogen layer and can be identified as the stretching and wagging modes of the SiH. The frequencies of these two modes are in excellent agreement with the experimental data but slightly shifted downwards in comparison to the frozen phonon calculation frequencies.

Naturally, the stretching mode 275 meV corresponds to the small amplitude frozen phonon calculation. The stretching frequency will shift down to about 270 meV when we include the zero point energy in an MD simulation. However, the wagging mode frequency is now shifted to 78 meV, whereas it was 74 meV in the frozen phonon calculation.

The most notable feature here is that a peak at 61 meV, as observed in the experiment, also shows up in the hydrogen overlayer vibration spectrum. We find that the polarization of this mode is entirely in-plane and propagates into the Si substrate layers.

Similar behavior is also found for Si(111):D. For the case of Si(111):D, there are three major peaks in the D layer in Figure 8.3, at 49, 70, and 197 meV. The 197 meV peak corresponds to the stretching mode and the 49 meV peak to the wagging mode, roughly scaled by $\sqrt{m_H/m_D}$. However, similar coupling leads to a shift in

the opposite direction.

The origin of the extra peak or surface resonance on the overlayer can be explained by considering the coupling between the wagging mode of SiH (or SiD) and a substrate mode originating from the TO(Γ) mode of bulk Si. On the Si(111) (1x1) termination, the TO(Γ) mode has uniform in-plane polarization and can couple to the wagging modes of the overlayer if their energies are close enough. By a frozen phonon calculation, we have found that the bare frequency of the TO(Γ) mode (without coupling to the overlayer) on a Si(111):H (or Si(111):D) slab is 67 meV in our model which is quite close to the bare wagging frequency of the SiH (74 meV) and of the SiD (52 meV). As the coupling is turned on, we expect the frequencies would shift as illustrated in Figure 8.4. In the Si(111):H system, the frequency of the wagging mode will shift up and the frequency of the surface resonance will shift down from their bare frequencies respectively. While in the Si(111):D system, the shift is in the opposite direction since the bare frequency of the wagging mode is lower than that of the TO(Γ) mode. The splitting between the wagging and the TO(Γ) modes should be expected to be larger in the case of Si(111):H and smaller in the case of Si(111):D since in the former case the two bare frequecies are much closer. This analysis is consistent with our lattice dynamical calculation and MD simulation results, and also with the experimental data.

We have also observed the frequency shift of the stretching mode as a function of the Si substrate temperature. For a comparison with the experiment, we have chosen to scale the MD temperature by

$$k_B T_{MD} = \int h\nu D(\nu)[\frac{1}{2} + \frac{1}{(e^{h\nu/k_B T} - 1)}]d\nu, \qquad (8.4)$$

where $D(\nu)$ is the phonon density of states of Si substrate. The result is summarized

in Figure 8.5 compared with the experiment [113]. The frequency shift is too large by a factor of about 1.5 compared to the experiment. The deviation may be due to the quantum nature of hydrogen, which cannot be simulated properly by a classical MD simulation. Also the linewidth (about 1.0 meV) is much broader than the experiment (about 0.25 meV). However when we calculate the velocity autocorrelation function of one H atom, then the linewidth is approximately 0.25 meV at 300 K. Although there is no surface reconstruction observed and the Si(111) substrate remains in (1×1) bulk termination, the H atom vibrations are sensitively affected by instantaneous thermal motion of Si atoms. It is very likely that if hydrogen were treated quantum mechanically, such instantaneous local deformations would not degrade the coherence of the H vibration as much. There is a similar frequency shift for the wagging mode of hydrogen in our MD simulation. These are summarized in Table 8.1.

-Related to the recent discussions about the sidepeaks to the stretching peak causing the peak intensity loss [113, 114], we think it is noteworthy that we have sidepeaks at frequencies $\nu_{str} \pm \nu_{wag}$ and $\nu_{str} - 2\nu_{wag}$ (Figure 8.6). The sidepeaks at $\nu_{str} \pm \nu_{wag}$ have polarization parallel to the surface, while the sidepeak at $\nu_{str} - 2\nu_{wag}$ is perpendicular to the surface. This indicates the existence of strong anharmonic coupling between the stretching and the wagging modes. The details of this coupling will be a subject of future investigations.

Summary

We have presented a model that can explain the existence of an additional peak in the EELS experiment. It is shown that the coupling of a hydrogen vibration mode with a bulk phonon mode in Si(111):H and Si(111):D surface is responsible

for the shift of the hydrogen vibration frequencies. This coupling of bulk phonon mode with an adatom vibration mode is important because usually the vibration frequency is used to identify the substrate-adatom geometric configuration. However, the calculated frequency shift and the linewidth of the stretching mode is larger than the experiment. It is likely that a quantum mechanical treatment of hydrogen may be necessary to pin down these anharmonic effects.

Table 8.1: The frequency (in meV) of the hydrogen stretching mode and wagging mode vs. silicon substrate temperature

T_{MD}	T_{scaled}	wagging mode	stretching mode
235	0	77.21	268.26
300	207	76.89	267.88
400	338	76.66	267.53
500	453	76.48	267.42
600	563	76.19	266.72

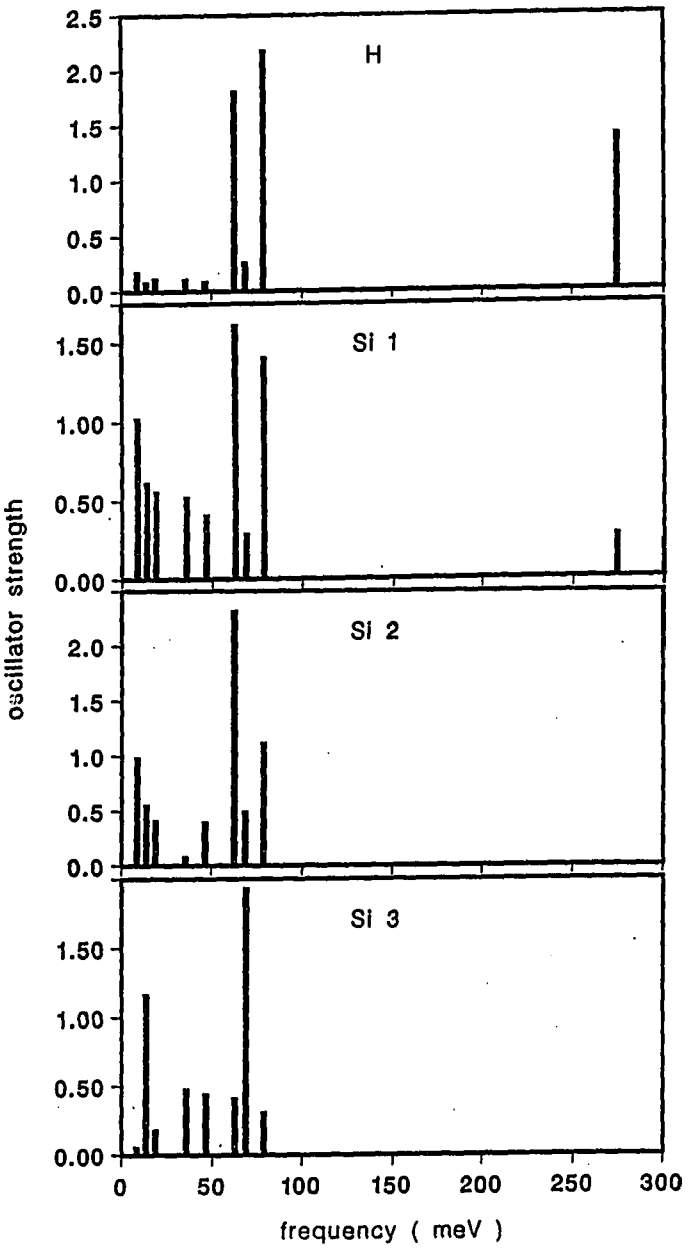

Figure 8.1: Normal mode strengths at the surface from the lattice dynamical calculation of Si(111):H

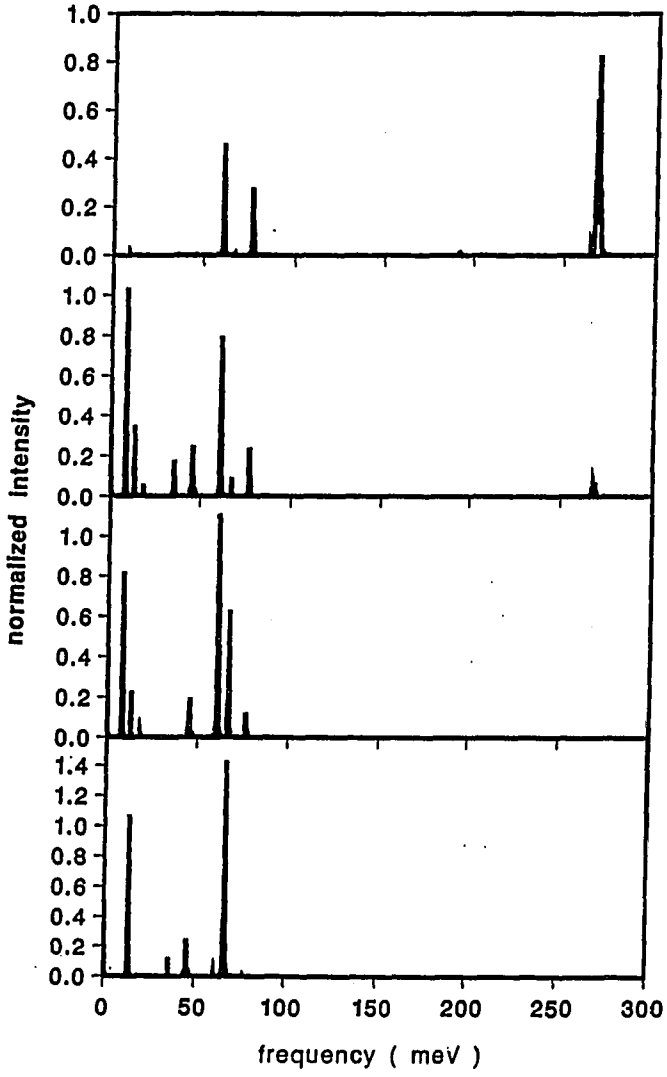

Figure 8.2: Phonon spectral intensity for the atoms in the H overlayer, first Si layer, second Si layer, and third Si layer from the top, respectively, calculated from the MD simulation

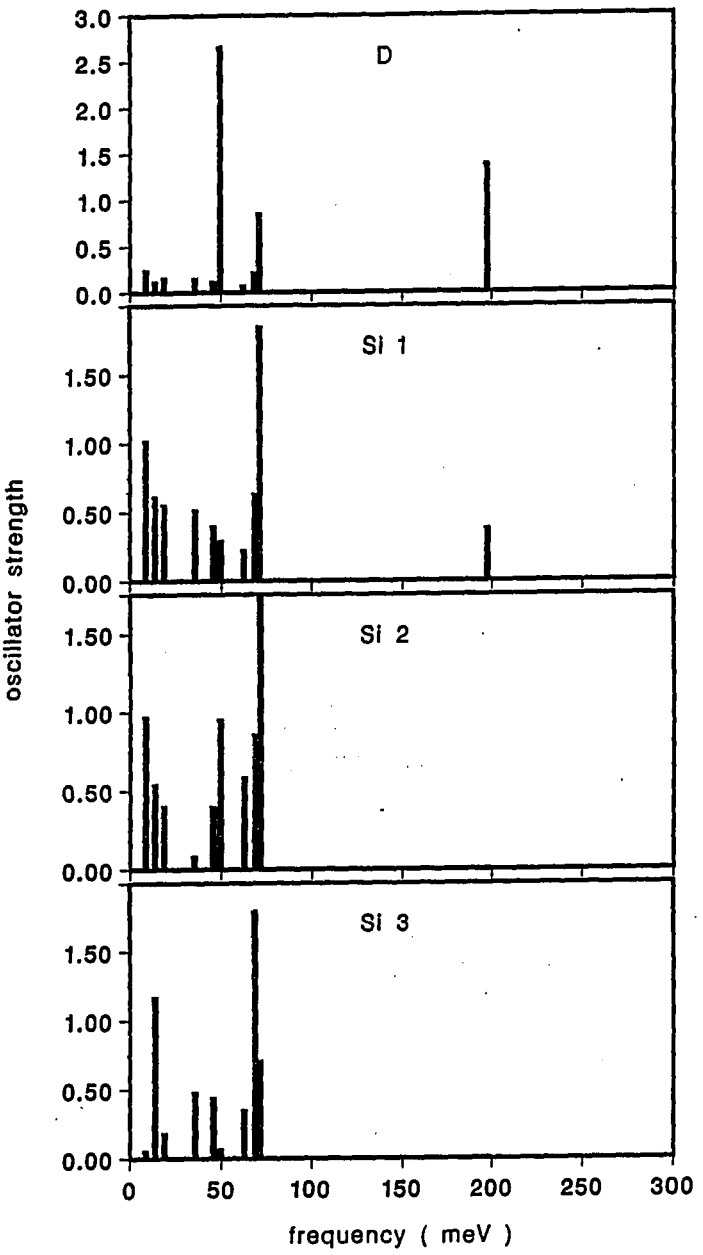

Figure 8.3: Normal mode strengths at the surface from the lattice dynamical calculation of Si(111):H

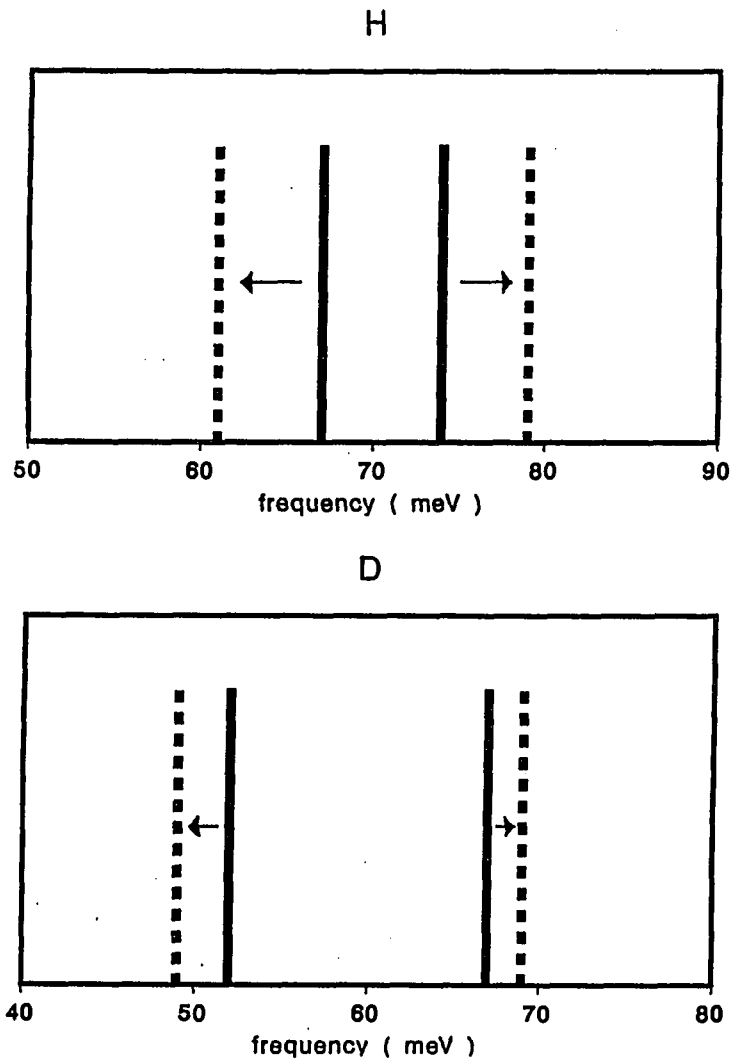

Figure 8.4: Schematic representation of the frequency shift caused by the coupling between the wagging mode and the Si substrate phonon from the lattice dynamical calculation. On top, the H wagging mode (74 meV) interacts with the Si substrate mode (68 meV). On bottom, the D wagging mode (52 meV) interacts with the same Si substrate mode (68 meV) resulting in the frequency shift in the opposite direction

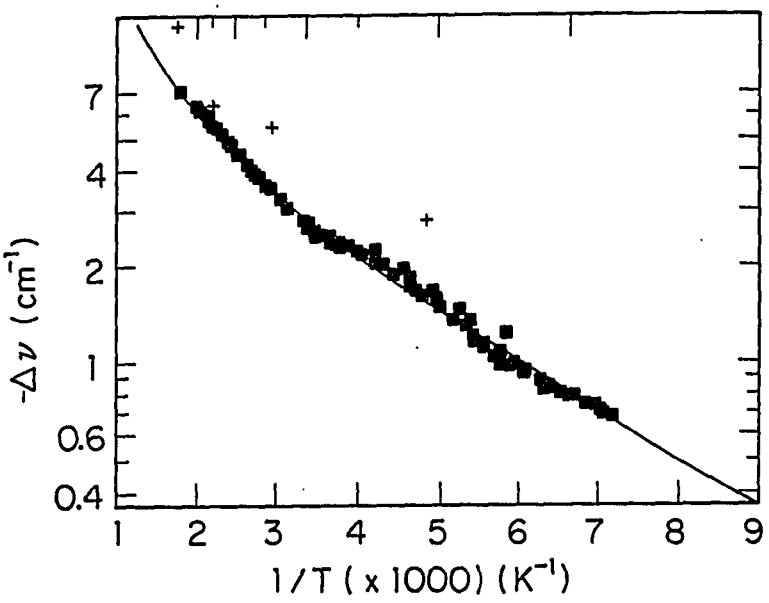

Figure 8.5: The frequency shift from the MD simulation (+) compared with the experiment

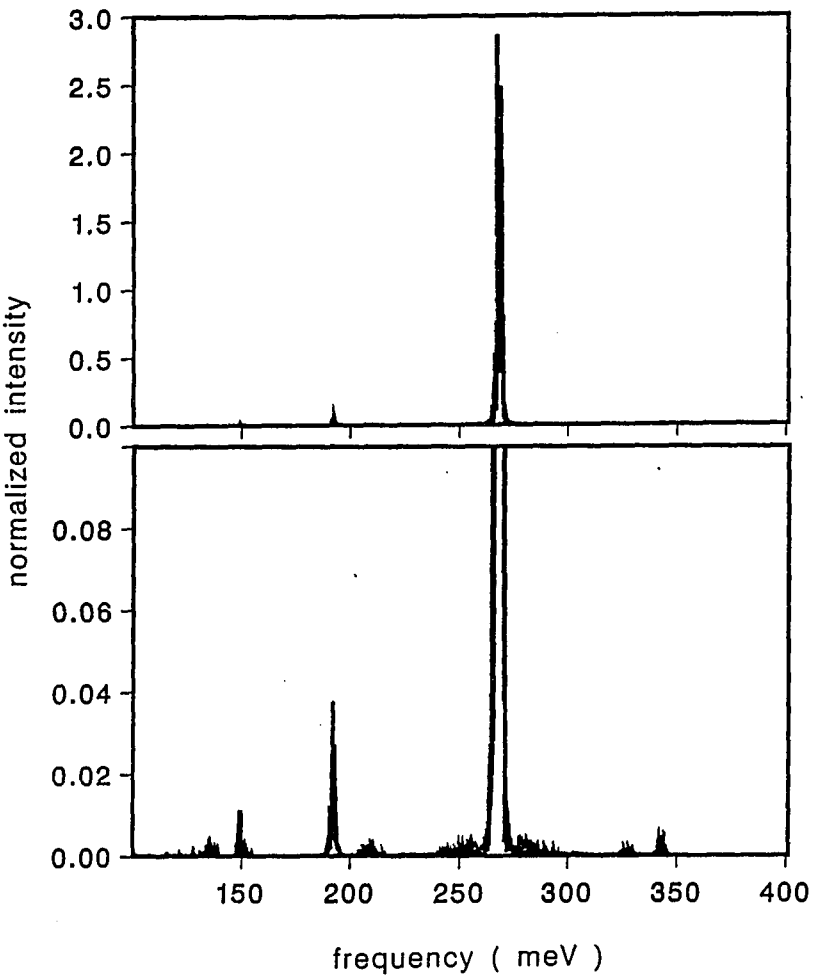

Figure 8.6: Phonon spectral intensity at T = 300 K showing sidepeaks to the H stretching mode

BIBLIOGRAPHY

[1] G. Alefeld, in *Hydrogen in Metals II*, Vol. 29 of *Topics in Applied Physics*, edited by J. Völkl and G. Alefeld (Springer, Berlin 1978), p. 1.

[2] Ch. A. Wert, in *Hydrogen in Metals II*, Vol. 29 of *Topics in Applied Physics*, edited by J. Völkl and G. Alefeld (Springer, Berlin 1978), p. 305.

[3] R. Wiswall, in *Hydrogen in Metals II*, Vol. 29 of *Topics in Applied Physics*, edited by J. Völkl and G. Alefeld (Springer, Berlin 1978), p. 201.

[4] K. W. Kehr, in *Hydrogen in Metals I*, Vol. 28 of *Topics in Applied Physics*, edited by J. Völkl and G. Alefeld (Springer, Berlin 1978), p. 197; J. Völkl and G. Alefeld, *ibid.*, p. 321.

[5] See, for example, A. Zangwill, *Physics at Surfaces*, (Cambridge University Press, Cambridge, 1988) p. 183.

[6] H. Wagner, in *Hydrogen in Metals I*, Vol. 28 of *Topics in Applied Physics*, edited by J. Völkl and G. Alefeld (Springer, Berlin 1978), p. 5.

[7] A. C. Switendick, in *Hydrogen in Metals I*, Vol. 28 of *Topics in Applied Physics*, edited by J. Völkl and G. Alefeld (Springer, Berlin 1978), p. 101.

[8] M. T. Yin and M. L. Cohen, Phys. Rev. Lett. **45**, 1004 (1980); Phys. Rev. B **26**, 5668 (1982).

[9] J. Ihm and J. D. Joannopoulos, Phys. Rev. B **24**, 4191 (1981); **26**, 4429 (1982).

[10] V. L. Moruzzi, J. F. Janak, and A. R. Williams, in *Calculated Electronic Properties of Metals*(Pergamon, New York, 1978).

[11] C.-L. Fu and K.-M. Ho, Phys. Rev. B **28**, 5480 (1983).

[12] K.-M. Ho, H.-J. Tao, and X.-Y. Zhu, Phys. Rev. Lett. **53**, 1586 (1984).

[13] D. A. Papaconstantopoulos and A. C. Switendick, J. Less-Common Met. **103**, 317 (1984).

[14] A. C. Switendick, J. Less-Common Met. **130**, 249 (1987),

[15] B. J. Min and K.-M. Ho, Phys. Rev. B **40**, 7532 (1989).

[16] P. Hohenberg and W. Kohn, Phys. Rev. **136**, B864 (1964); W. Kohn and L. J. Sham, Phys. Rev. **140**, A1133 (1965); For a review, see, for example, R. O. Jones and O. Gunnarsson, Rev. Mod. Phys. **61**, 689 (1989).

[17] For example see a review article by W. E. Pickett, Comp. Phys. Rep. **9**, 115 (1989).

[18] D. R. Hamann, M. Schlüter, and C. Chiang, Phys. Rev. Lett. **43**, 1494 (1979).

[19] E. Wicke, H. Brodowsky, and H. Züchner, "Hydrogen in Palladium and Palladium Alloys", in *Hydrogen in Metals I. Basic Properties*, G. Alefeld and J.Völkl, eds., Topics in Applied Physics, Vol. 28 (Springer, Berlin, Heidelberg, New York 1978).

[20] L. J. Gillespie and W. R. Downs, J. Am. Chem. Soc. **61**, 2496 (1939).

[21] J. C. Phillips and L. Kleinman, Phys. Rev. **116**, 287 (1959).

[22] See, for example, M. L. Cohen and V. Heine, Solid State Physics **24**, 37 (1970).

[23] G. P. Kerker, J. Phys. C. **13**, L189 (1980).

[24] D. Vanderbilt, Phys. Rev. B **32**, 8412 (1985).

[25] A. M. Rappe, K. M. Rabe, E. Kaxiras, and J. D. Joannopoulos, Phys. Rev. B **41**, 1227 (1990).

[26] N. Troullier and J. L. Martins, Phys. Rev. B **43**, 1993 (1991).

[27] D. Vanderbilt, Phys. Rev. B **41**, 7892 (1990).

[28] L. Hedin and B. I. Lundqvist, J. Phys. C. **4**, 2064 (1971).

[29] D. D. Koelling and B. N. Harmon, J. Phys. C. **10**, 3107 (1977).

[30] S. G. Louie, S. Froyen, and M. L. Cohen, Phys. Rev. B **26**, 1738 (1982).

[31] E. Wigner, Phys. Rev. **46**, 1002 (1934).

[32] J. Perdew and A. Zunger, Phys. Rev. B **23**, 5048 (1980); C. M. Ceperly and B. J. Alder, Phys. Rev. Lett. **45**, 566 (1980).

[33] J. Ihm, A. Zunger, and M. L. Cohen, J. Phys. C:Solid State Phys. **12**, 4409 (1979).

[34] P. P. Ewald, Ann. Physik **64**, 253 (1921); K. Fuchs, Proc. Roy. Soc. (London) A**151**, 585 (1935).

[35] S. G. Louie, K. M. Ho, and M. L. Cohen, Phys. Rev. B **19**, 1774 (1979).

[36] D. Khatamian, C. Stassis, and B. J. Beaudry, Phys. Rev. B **23**, 624 (1981).

[37] D. L. Anderson, R. G. Barnes, S. O. Nelson, and D. R. Torgeson, Phys. Lett. A **74**, 427 (1979).

[38] J. E. Bonnet, C. Juckum, and A. Lucasson, J. Phys. F **12**, 699 (1982).

[39] J. E. Bonnet, S. K. P. Wilson, and D. K. Ross, in *Proceedings of International Symposium on the Electronic Structure and Properties of Hydrogen in Metals, Richmond, Virginia, 1982*, edited by P. Jena and C. B. Satterthwaite (Plenum, New York, 1983).

[40] P. G. Dantzer and O. J. Kleppa, J. Chem. Phys. **73**, 5259 (1980).

[41] I.S.Anderson, J.J.Rush, T.Udovich, and J.M.Rowe, Phys. Rev. Lett. **57**,2822(1986).

[42] B. J. Beaudry and K. A. Gschneidner, Jr., in *Handbook on the Physics and Chemistry of Rare Earths*, edited by K. A. Gschneidner, Jr. and L. R. Eyring (North Holland, Amsterdam, 1978).

[43] J. H. Rose, J.Ferrante, and J. R. Smith, Phys. Rev. Lett. 47, 675 (1981).

[44] W. A. Grosshans, Y. K. Vohra, and W. B. Holzapfel, Phys. Rev. Lett. **49**, 1572 (1982); Y. K. Vohra, V. Vijayakumar, B. K. Godwal, and S. K. Sikka, Phys. Rev. B **30**, 6205 (1984).

[45] W. J. Carter, J. N. Fritz, S. P. Marsh, and A. J. McQueen, J. Phys. Chem. SOlids **36**, 741 (1975).

[46] T. E. Scott, in *Handbook on the Physics and Chemistry of Rare Earths*, edited by K. A. Gschneidner, Jr. and L. R. Eyring (North Holland, Amsterdam, 1978).

[47] D. E. Eastman, Solid State Commun. **7**, 1697 (1969).

[48] T. L. Loucks, Phys. Rev. **144**, 504 (1966).

[49] B. J. Beaudry and F. H. Spedding, Metall. Trans. B **6**, 419 (1975).

[50] O. Gunnarson and P. Johansson, Int. J. Quantum Chem. **X**, 307 (1976).

[51] L. N. Yannopoulos, R. K. Edwards, and P. G. Wahlbeck, J. Phys. Chem. **69**, 2510 (1965).

[52] J. E. Bonnet, C. Juckum, and A. Lucasson, J. Phys. F: Met. Phys. **12**, 699 (1982).

[53] I.S.Anderson, J.J.Rush, T.Udovich and J.M.Rowe, Phys. Rev. Lett. **57**,2822(1986).

[54] I. S. Anderson, N. F. Berk, J. J. Rush, and T. J. Udovic, Phys. Rev. B **37**, 4358 (1988).

[55] O. N. Carlson, F. A. Schmidt, and D. T. Peterson, J. Less-Common Met. **10**, - 1 (1966).

[56] D. L. Anderson, R. G. Barnes, S. O. Nelson, and D. R. Torgeson, Phys. Lett. **74A**, 427 (1979).

[57] L. Lichty, R. J. Schoenberger, D. R. Torgeson and R. G. Barnes, J. of the Less-Common Metals **129**, 31 (1987).

[58] I. S. Anderson, A. Heidemann, J. E. Bonnet, D. K. Ross, S. K. P. Wilson, and M. W. McKergow, J. Less-Common Met. **101**,405 (1984).

[59] I. S. Anderson, D. K. Ross, and J. E. Bonnet, Z. Phys. Chem. Neue Folge **164**, S923 (1989).

[60] M. W. McKergow, D. K. Ross, J. E. Bonnet, I. S. Anderson, and O. Schaerpf, J. Phys. C: Solid State Phys. **20**, 1909 (1987).

[61] F. Liu, M. Challa, S. N. Khanna, and P. Jena, Phys. Rev. Lett. **63**, 1396 (1989).

[62] O. Blaschko, G. Krexner, J. N. Daou, and P. Vajda, Phys. Rev. Lett. **55**,2876 (1985); O. Blaschko, G. Krexner, J. Pleischiutschnig, J. N. Daou, and P. Vajda, Phys. Rev. B **39**, 5605 (1989).

[63] O. Blaschko, J. Pleischiutschnig, P. Vajda, J. P. Burger, and J. N. Daou, Phys. Rev. B **40**, 5344 (1989).

[64] S. Prakash, J. E. Bonnet, and P. Lucasson, J. Less-Common Met. **68**, 1 (1979).

[65] C. A. Swenson, unpublished.

[66] C. Elsässer, N. Takeuchi, K. M. Ho, C. T. Chan, P. Braun, and M. Fähnle, J. Phys. Condens. Matter **2**, 4371 (1990).

[67] K. A. Gschneidner, Jr., H. Gnugesser and K. Neumaier, Physica **108B**, 1007 (1981)

[68] I. Svare, D. R. Torgeson, and F. Borsa, Phys. Rev. B **43**, 7448 (1991).

[69] S. M. Bennington, M. J. Benham, D. K. Ross, A. D. Taylor, and Z. A. Bowden, Z. Phys. Chem. Neue Folge **164**, 1071 (1989).

[70] I. S. Anderson, N. F. Berk, J. J. Rush, T. J. Udovic, R. G. Barnes, A. Magerl, and D. Richter, Phys. Rev. Lett. **65**, 1439 (1990).

[71] J. Völkl, H. Wipf, B. J. Beaudry, and K. A. Gschneidner, Jr., Phys. Stat. Sol. B **144**, 315 (1987).

[72] C. P. Flynn and A. M. Stoneham, Phys. Rev. B **1**, 3966 (1970); Yu. Kagan and M. I. Klinger, J. Phys. C **7**, 2791 (1974); D. Emin, M. I. Baskes, and W. D. Wilson, Phys. Rev. Lett. **42**, 791 (1979); R. Hempelmann, J. Less-Common Met. **101**, 69 (1984).

[73] D. Khatamian, J. Less-Common Met. **129**, 153 (1987).

[74] R. Car and M. Parrinello, Phys. Rev. Lett. **55**, 2471 (1985).

[75] D. J. Chadi, Phys. Rev. Lett. **41**, 1062 (1978); Phys. Rev. B **29**, 785 (1984); Phys. Rev. Lett. **59**, 1691 (1988).

[76] W. A. Harrison, *Electronic Structure and the Properties of Solids*, W. H. Freeman and Company, San Francisco (1980).

[77] D. Tomanék and M. A. Schlüter, Phys. Rev. Lett. **56**, 1055 (1986); Phys. Rev. B **36**, 1208 (1987).

[78] D. G. Allan and E. J. Mele, Phys. Rev. Lett. **53**, 826 (1984); O. L. Alerhand, D. G. Allan, and E. J. Mele, Phys. Rev. Lett. **55**, 2700 (1985).

[79] F. S. Khan and J. Q. Broughton, Phys. Rev. B **39**, 3688 (1989).

[80] M. Menon and R. E. Allen, Phys. Rev. B **33**, 7099 (1986); *ibid.* **38**, 6196 (1988).

[81] J. C. Slater and G. F. Koster, Phys. Rev. **94**, 1498 (1954).

[82] C. Z. Wang, C. H. Xu, C. T. Chan, and K. M. Ho, Bull. Am. Phys. Soc. **36**, 421 (1991).

[83] C. Z. Wang, C. T. Chan, and K. M. Ho, Phys. Rev. B **39**, 8586 (1989); Phys. Rev. B **40**, 3390 (1989). Phys. Rev. B **42**, 11276 (1990).

[84] P. N. Keating, Phys. Rev. **145**, 637 (1966).

[85] F. H. Stillinger and T. A. Weber, Phys. Rev. B **31**, 5262 (1985).

[86] R. Biswas and D. R. Hamann, Phys Rev. B **36**, 6434 (1987).

[87] J. Tersoff, Phys. Rev. Lett. **56**, 632 (1986).

[88] For example, see review article by S. J. Pearton, J. W. Corbett, and T. S. Shi, Appl. Phys. A **43**, 153 (1987).

[89] H. Ubara, T. Imura, and A. Hiraki, Solid State Commun. **50**, 673 (1984); M. Grundner and H. Jacob, Appl. Phys. A **39**, 73 (1986); E. Yablonovitch, D. L. Allara, C. C. Chang, T. Gmitter, and T. B. Bright, Phys. Rev. Lett. **57**, 249 (1986). G. S. Higashi, Y. J. Chabal, G. W. Trucks, and K. Raghavachari, Appl. Phys. Lett. **56**, 656 (1990).

[90] For example, see review article by D. Haneman, Rep. Prog. Phys. **50**, 1045 (1987) and the references therein.

[91] B. Zhang, C. T. Chan, and K. M. Ho, unpublished.

[92] K. J. Chang and D. J. Chadi, Phys. Rev. Lett. **60**, 1422 (1980); Phys. Rev. B. **40**, 11644 (1989).

[93] C. G. Van de Walle, Y. Bar-Yam, and S. T. Pantelides, Phys. Rev. Lett. **60**, 2761 (1988); C. G. Van de Walle, P. J. H. Denteneer, Y. Bar-Yam, and S. T. Pantelides, Phys. Rev. B **39**, 10791 (1989).

[94] E. Kaxiras and J. D. Joannopoulos, Phys. Rev. B **37**, 8842 (1988).

[95] F. Buda, G. L. Chiarotti, R. Car, and M. Parrinello, Phys. Rev. Lett. **63**, 294 (1989).

[96] L. Guttman, Phys. Rev. B **23**, 1866 (1981); L. Guttman and C. Y. Fong, Phys. Rev. B **26**, 6756 (1982).

[97] A. Selmani, D. R. Salahub, and A. Yelon, Surf. Sci. **202**, 269 (1988).

[98] L. J. Lewis, N. Mousseau, and F. Drolet, in *Atomic-Scale Calculations in Materials Science*, Vol. 144 of *Materials Research Society Symposium Proceedings*, edited by J. Tersoff, D. Vanderbilt, and V. Vitek, (MRS, Pittsburgh, 1989); N. Mousseau and L. J. Lewis, Phys. Rev. B **41**, 3702 (1990).

[99] C. W. Gear, The numerical integration of ordinary differential equations of various orders, Report ANL 7126, Argonne National Laboratory, (1966); C. W. Gear, *Numerical initial value problems in ordinary differential equations*, Prentice-Hall, Englewood Cliffs, NJ (1971).

[100] W. F. van Gunsteren and H. J. C. Berendsen, Mol. Phys. **34**, 1311 (1977).

[101] J. C. Slater and G. F. Koster, Phys. Rev. **94**, 1498 (1954).

[102] D. C. Allan and E. J. Mele, Phys. Rev. Lett. **53**, 826 (1984); Phys. Rev. B. **35**, 5533 (1987).

[103] D. C. Allan and E. J. Mele, Phys. Rev. B **31**, 5565 (1985).

[104] S. R. Gunn and L. G. Green, J. Phys. Chem. **65**, 779 (1961); D. S. Horowitz and W. A. Goddard III, J. Mol. Struct. **163**, 207 (1988).

[105] G. Lucovsky, R. J. Nemanich, and J. C. Knights, Phys. Rev. B **19**, 2064 (1979).

[106] K. M. Ho and M. L. Cohen, Phys. Rev. B **15**, 3888 (1977).

[107] See a review article by M. Cardona, Phys. Stat. Sol. B **118**, 463 (1983).

[108] H. Froitzheim, H. Lammering, and H.-L. Günter, Phys. Rev. B **27**, 2278 (1983).

[109] H. Froitzheim, U. Köhler, and H. Lammering, Surf. Sci. **149**, 537 (1985).

[110] J. A. Schaefer, F. Stucki, J. A. Anderson, G. J. Lapeyre, and W. Göpel, Surf. Sci. **140**,207, (1984).

[111] U. Harten, J. P. Toennies, Ch. Wöll, L. Miglio, P. Ruggerone, L. Colombo, and G. Benedek, Phys. Rev. B **38**, 3305 (1988).

[112] J. C. Phillips, Phys. Rev. **166**, 832 (1968); R. M. Martin, Phys. Rev. **186**, 871 (1969); W. Weber, Phys. Rev. B **15**, 4789 (1977).

[113] P. Dumas, Y. J. Chabal, and G. S. Higashi, Phys. Rev. Lett. **65**, 1124 (1990); P. Guyot-Sionnest, P. Dumas, Y. J. Chabal, and G. S. Higashi, Phys. Rev. Lett. **64**, 2156 (1990); P. Guyot-Sionnest,Phys. Rev. Lett. **66**, 1489 (1991).

[114] P. Dumas, Y. J. Chabal, and G. S. Higashi, J. Electron Spectroscopy and Related Phenomena, **54/55**, 103 (1990).